

# Deep Jump Gaussian Processes for Surrogate Modeling of High-Dimensional Piecewise Continuous Functions

**Yang Xu**

*Industrial & Systems Engineering  
University of Washington, Seattle, WA, USA*

YXU59@UW.EDU

**Chiwoo Park**

*Industrial & Systems Engineering  
University of Washington, Seattle, WA, USA*

CHIWPARK@UW.EDU

**Editor:**

## Abstract

We introduce Deep Jump Gaussian Processes (DJGP), a novel method for surrogate modeling of high-dimensional piecewise continuous functions. DJGP overcomes the limitations of conventional Jump Gaussian Processes in high-dimensional input spaces by adding a locally linear projection layer to Jump Gaussian Processes. This projection uses region-specific matrices to capture local subspace structures, naturally complementing the localized nature of JGP, a variant of local Gaussian Processes. To control model complexity, we place a Gaussian Process prior on the projection matrices, allowing them to evolve smoothly across the input space. The projected inputs are then modeled with a JGP to capture piecewise continuous relationships with the response. This yields a distinctive two-layer deep learning of GP/JGP. We further develop a scalable variational inference algorithm to jointly learn the projection matrices and JGP hyperparameters. Experiments on synthetic and benchmark datasets demonstrate that DJGP delivers superior predictive accuracy and more reliable uncertainty quantification compared to existing approaches.

**Keywords:** Gaussian process, piecewise continuous surrogates, local projection, variational inference

## 1. Introduction

This paper addresses surrogate modeling of piecewise continuous system responses in high-dimensional input spaces. In many engineering and scientific domains, system responses can exhibit abrupt jumps or sharp transitions under small input perturbations. For instance, in geostatistics, subsurface rock properties such as porosity and permeability can change dramatically at sedimentary interfaces, naturally giving rise to piecewise continuous behavior (Chiles and Delfiner, 2012). In materials science, first-order phase transitions (e.g., the ferromagnetic–paramagnetic shift at the Curie point) induce discontinuous changes in properties like magnetization and density (Park et al., 2022). In econometrics, regression discontinuity designs leverage sharp outcome changes at policy thresholds or eligibility cutoffs to identify causal effects (Kang et al., 2019). Developing surrogate models for piecewise continuous response surfaces is therefore essential for data-driven understanding and reliable uncertainty quantification of such systems.

While Gaussian processes (GPs) offer a flexible Bayesian nonparametric surrogate model with uncertainty quantification capability, they typically rely on stationary kernels—such as the squared exponential—which assume that function behavior is homogeneous across the input space. These

kernels induce strong correlations between nearby inputs and impose global smoothness, making them poorly suited for modeling abrupt changes or discontinuities (Qiu, 2009).

Nonstationary GP models can better adapt these changes by adjusting their hyperparameters locally to capture varying covariance structures (Sampson and Guttorp, 1992; Sauer et al., 2023b). Representative approaches include heteroskedastic GPs (Kersting et al., 2007; Quadrianto et al., 2009) and latent GPs that model kernel parameters such as variance or lengthscale (Paciorek and Schervish, 2003; Tolvanen et al., 2014; Heinonen et al., 2016). A more flexible alternative is Deep Gaussian Processes (DGPs) (Lawrence and Moore, 2007; Damianou and Lawrence, 2013), which stack multiple GP layers to warp inputs into nonlinear feature spaces and map them to responses. This hierarchical structure enables DGPs to capture complex nonstationary patterns that shallow GPs cannot represent, but that comes with the cost of intractable inferences. Considerable effort has gone into scalable inference for DGPs, including Vecchia approximations (Sauer et al., 2023a), variational frameworks (Titsias, 2009; Hensman et al., 2013; Damianou et al., 2011; Damianou, 2015), and sampling-based methods (Havasi et al., 2018). Hybrid models that combine neural network layers with GP layers further improve flexibility and scalability (Dai et al., 2015; Wilson et al., 2016b,a; Lee et al., 2017). Despite these advances, most nonstationary GP models—including DGP-based variants—remain fundamentally smooth and tend to blur discontinuities, while DGPs in particular are often data-hungry and require large training sets.

An approach directly suited for modeling piecewise continuous surrogates is the partitioned GP, which divides the input space into regions and fits an independent GP within each region. When the partitions align well with discontinuities, partitioned GPs can effectively represent piecewise continuous surrogates. To control model complexity and computational cost, existing methods typically constrain how the space is partitioned. Common approaches include tessellation-based methods (e.g., Voronoi diagrams) (Kim et al., 2005; Pope et al., 2021; Luo et al., 2021) and treed partitioning (Gramacy and Lee, 2008; Konomi et al., 2014; Taddy et al., 2011). These approaches improve scalability but often rely on axis-aligned or overly simplistic splits, making them less effective for complex or nonlinear boundaries.

A recent and more flexible approach is the Jump Gaussian Process (JGP) (Park, 2022). Rather than explicitly modeling a global partition of the input space, JGP constructs local approximations of the partition boundaries. If the boundary is sufficiently smooth, it can be locally approximated by a linear or low-order polynomial function. At each test location, JGP fits both the local polynomial boundary and the local GP parameters using data with a small neighborhood of the test location. By leveraging these local approximations, JGP can represent piecewise continuous surrogates with highly complex regional boundaries. However, JGP faces challenges in high-dimensional settings. As input dimensionality increases, data sparsity grows, requiring larger neighborhoods to obtain sufficient local training data. This leads to coarser approximations and ultimately limits JGP’s ability to capture fine-grained local structures in high-dimensional spaces.

The limitations of JGP motivate us to investigate dimensionality reduction for JGP. An easy fix of the dimensionality issue may be to apply dimensionality reduction prior to GP modeling, e.g. linear technique such as Principal Component Analysis (PCA) (Abdi and Williams, 2010), nonlinear technique such as kernel PCA (Schölkopf et al., 1997), Isomap (Balasubramanian and Schwartz, 2002), local linear embedding (Saul and Roweis, 2000), autoencoders (Wang et al., 2016), or t-SNE (Maaten and Hinton, 2008). However, these methods are unsupervised, meaning that they rely only on input data and ignore correlations between transformed features and the response variable. A better approach can be to use supervised approaches such as Sliced Inverse Regression (SIR) (Li, 1991),

supervised autoencoders (Makhzani and Frey, 2015; Le et al., 2018) and conditional variational autoencoders (CVAEs) (Sohn et al., 2015; Kingma et al., 2014). Nevertheless, these supervised dimension-reduction techniques are still not optimized from the downstream GP modeling task.

Dimensionality reduction can also be optimized directly for a target GP modeling task. For instance, the Mahalanobis Gaussian Process (MGP) (AUEB et al., 2013) learns a linear projection of the inputs to a low dimensional space, where the linear projection matrix is optimized jointly with the GP model parameters. The Gaussian Process Latent Variable Model (GP-LVM) (Titsias and Lawrence, 2010) generalizes the linear projection with a nonlinear projection represented by a GP model, resulting in two-layer GP model with the first layer for non-linear feature mapping and the second layer for mapping to the response variable. The Deep Mahalanobis Gaussian Process (DMGP) (de Souza et al., 2022) extends MGP with a similar two-layer design. It introduces a distinct linear projection matrix for each input location, with GP priors enforcing smooth variation of these matrices across the input space. The projected features are then passed to another GP layer to model the response.

Nevertheless, existing built-in dimensionality reduction methods are not tailored for JGP. Their integration is nontrivial due to a fundamental modeling difference: conventional GP models follow an inductive learning paradigm, whereas JGP operates in a transductive setting—fitting a local model at each test location. The goal of this paper is to develop a built-in dimensionality reduction approach specifically designed for JGP, yielding a piecewise continuous surrogate model that remains effective in high-dimensional input spaces.

Our approach adopts a locally linear projection from high-dimensional inputs to low-dimensional latent features. For each test location, we introduce a separate linear projection matrix that maps the inputs to latent features, while enforcing spatial correlations among these projection matrices through a GP prior. The resulting local latent features are then mapped to the response variable using a JGP model, forming a novel local two-layer GP/JGP architecture. To enable scalable inference, we develop a variational algorithm that jointly optimizes both layers. We refer to this framework as the Deep Jump Gaussian Processes (DJGP).

The remainder of this paper is organized as follows. Section 2 reviews relevant background on Stationary GP, Jump GP and Mahalanobis GP. In Section 3, we introduce the proposed DJGP model and its variational inference scheme. Section 3.2 details the full variational inference procedure. Section 4 presents numerical evaluation with synthetic datasets, and an extensive hyperparameter sensitivity analysis that provides practical guidelines for model configuration. In Section 5, we evaluate the proposed model on real-world datasets. Finally, Section 6 concludes the paper with a summary and discussion of future directions.

## 2. Review

Here we provide a brief technical review to the key technical components: Stationary GP, Jump GP and Mahalanobis GP.

### 2.1 Stationary Gaussian Process (GP) Surrogates

Consider an unknown function  $f : \mathcal{X} \rightarrow \mathbb{R}$  to relate an input  $\mathbf{x} \in \mathcal{X}$  to a real response  $y$ , where  $\mathcal{X} \subset \mathbb{R}^D$  denote the input space. We can build a stationary GP surrogate to  $f$  given its noisy

evaluations,

$$y_i \stackrel{\text{i.i.d.}}{\sim} \mathcal{N}(f(\mathbf{x}_i), \sigma^2), \quad i = 1, \dots, N,$$

where a prior distribution over  $f$  is defined by the stationary Gaussian process with a constant mean function  $\mu$  and covariance kernel  $c(\cdot, \cdot)$ ,

$$f(x) \sim \mathcal{GP}(\mu, c(\cdot, \cdot; \theta)).$$

The covariance kernel is a positive definite function  $c : \mathcal{X} \times \mathcal{X} \rightarrow \mathbb{R}$  parameterized by hyperparameters  $\theta$ . A common modeling assumption on the kernel is stationarity, where the covariance kernel depends only on the relative distance between inputs. A widely used stationary kernel is the squared exponential (SE):

$$k_{\text{SE}}(\mathbf{x}_i, \mathbf{x}_j; \sigma_f, \ell_1, \dots, \ell_D) = \sigma_f^2 \exp\left(-\frac{1}{2} \sum_{m=1}^D \frac{(x_{im} - x_{jm})^2}{\ell_m^2}\right), \quad (1)$$

where  $x_{im}$  denotes the  $m$ th dimension of  $\mathbf{x}_i$ . The Matérn class provides greater flexibility by controlling the smoothness of the function (Wendland, 2004).

Under this prior, the vector of the observed outputs  $\mathbf{y}_N = [y_1, \dots, y_N]^\top$  follows a multivariate normal distribution,

$$\mathbf{y}_N \sim \mathcal{N}(\mu \mathbf{1}_N, \sigma^2 \mathbf{I}_N + \mathbf{C}_N),$$

where  $\mathbf{C}_N$  is a  $N \times N$  matrix with its  $(i, j)$ th element equal to  $c(\mathbf{x}_i, \mathbf{x}_j; \theta)$ ,  $\mathbf{1}_N$  is a  $N$ -dimensional column vector of ones, and  $\mathbf{I}_N$  is a  $N$ -dimensional identity matrix.

The hyperparameters  $\theta$ , mean parameter  $\mu$ , and noise variance  $\sigma^2$ —can be learned by maximizing the log marginal likelihood:

$$L(\theta, \mu, \sigma^2) = -\frac{1}{2}(\mathbf{y}_N - \mu \mathbf{1}_N)^\top [\sigma^2 \mathbf{I}_N + \mathbf{C}_N]^{-1} (\mathbf{y}_N - \mu \mathbf{1}_N) - \frac{1}{2} \log |\sigma^2 \mathbf{I}_N + \mathbf{C}_N| - \frac{N}{2} \log(2\pi),$$

using either gradient-based optimization or EM-style iterative schemes, depending on the model setting (Santner et al., 2003; Gramacy, 2020; Titsias, 2009). We use the hat notations  $\hat{\mu}, \hat{\theta}, \hat{\sigma}^2$  to denote the estimated parameters.

Given the parameter estimates, we can derive the predictive distribution of  $f$  at a test input  $\mathbf{x}^{(*)} \in \mathcal{X}$ . The joint distribution of  $\mathbf{y}_N$  and an unknown testing output  $y(\mathbf{x}^{(*)})$  is a multivariate normal (MVN) distribution. Applying the simple Gaussian conditioning formula gives the posterior predictive distribution of  $y(\mathbf{x}^{(*)})$ , which is also Gaussian with the following predictive mean and variance:

$$\begin{aligned} \mathbb{E}[y(\mathbf{x}^{(*)})] &= \hat{\mu} + \mathbf{k}_N^\top [\hat{\sigma}^2 \mathbf{I}_N + \mathbf{C}_N]^{-1} (\mathbf{y}_N - \hat{\mu} \mathbf{1}_N), \\ \text{Var}(y(\mathbf{x}^{(*)})) &= c(\mathbf{x}^{(*)}, \mathbf{x}^{(*)}; \hat{\theta}) - \mathbf{c}_N^\top [\hat{\sigma}^2 \mathbf{I}_N + \mathbf{C}_N]^{-1} \mathbf{c}_N, \end{aligned}$$

where  $\mathbf{c}_N = [c(\mathbf{x}_i, \mathbf{x}^{(*)}; \hat{\theta}) : i = 1, \dots, N]$  is a  $N \times 1$  vector of the covariance values between the training data and the test data point.

The stationary GP model has many advantages such as modeling flexibility, analytical solution form and uncertainty quantification capability. Despite them, Gaussian Processes (GPs) scale poorly with data size, requiring  $\mathcal{O}(N^3)$  time and  $\mathcal{O}(N^2)$  memory, which limits their applicability to moderately sized datasets. Moreover, in many practical settings, the underlying regression function is piecewise continuous and exhibits abrupt changes across unknown boundaries—behavior that stationary GPs are ill-equipped to model. Standard kernels impose global smoothness assumptions,

leading to spurious correlations across discontinuities and biased estimates near regime shifts. Since stationary kernels depend solely on pairwise distances, they struggle to capture abrupt changes or heteroscedastic patterns. The Jump Gaussian Process (JGP) (Park, 2022) addresses these limitations.

## 2.2 Jump Gaussian Processes (JGP)

JGP is best understood through the lens of local GP modeling (LAGP; Gramacy and Apley, 2015). For each test location  $x^{(*)}$ , a small subset of nearby training data is selected,  $\mathcal{D}_n^{(*)} = \{(\mathbf{x}_i^{(*)}, y_i^{(*)})\}_{i=1}^n$ , and a conventional stationary GP model is fitted to this local data. This approach is computationally efficient— $O(n^3)$  versus  $O(N^3)$  when  $n \ll N$ —and can be massively parallelized across many test points (Gramacy et al., 2014). A key limitation of LAGP in estimating piecewise continuous surrogates is that local neighborhoods  $\mathcal{D}_n^{(*)}$  may overlap partially or fully with discontinuities. In such cases, LAGP can yield biased predictions (Park, 2022) because the local data may mix training examples drawn from regions of the input space separated by abrupt regime shifts.

JGP addresses this issue by explicitly dividing the local data into two groups by regime shifts: data in the same regime as the test input  $\mathbf{x}^{(*)}$  and the remainder. To accomplish this, JGP introduces a latent binary random variable  $v_i^{(*)} \in \{0, 1\}$  indicating whether a training input  $\mathbf{x}_i^{(*)}$  belongs to the same regime as  $\mathbf{x}^{(*)}$  ( $v_i^{(*)} = 1$ ) or not ( $v_i^{(*)} = 0$ ). Conditional on  $v_i^{(*)}$  values,  $i = 1, \dots, n$ , the local data  $\mathcal{D}_n^{(*)}$  is partitioned into two groups:  $\mathcal{D}_* = \{i \in \{1, \dots, n\} : v_i^{(*)} = 1\}$  and  $\mathcal{D}_o = \{1, \dots, n\} \setminus \mathcal{D}_*$ .

Only  $\mathcal{D}_*$  contributes to predicting  $f$  at  $x^{(*)}$ , while data in  $\mathcal{D}_o$  are down-weighted via a uniform “outlier” likelihood. The full specification is completed by modeling  $\mathcal{D}_*$  with a stationary GP [Section 2.1],  $\mathcal{D}_o$  with dummy likelihood  $p(y_i^{(*)} | v_i^{(*)} = 0) \propto u$  for some constant,  $u$ , and assigning a prior to the latent variable  $v_i^{(*)}$ , via a sigmoid function  $\pi$  applied to a partitioning function  $g(\mathbf{x}, \boldsymbol{\omega})$ ,

$$p(v_i^{(*)} = 1 | \mathbf{x}_i^{(*)}, \boldsymbol{\nu}) = \pi(h(\mathbf{x}_i^{(*)}, \boldsymbol{\nu})), \quad (2)$$

where  $\boldsymbol{\nu}$  is another hyperparameter. The choice of the parametric partitioning function  $h$  determines the boundary separating  $\mathcal{D}_o$  and  $\mathcal{D}_*$ . At the local level, linear or quadratic forms of  $h$  serves good Taylor approximations to complex domain boundaries. For further details, see the original JGP paper (Park, 2022). In this work, we adopt the linear form  $h(\mathbf{x}) = \boldsymbol{\nu}^T [1, \mathbf{x}]$ .

Specifically, for  $\boldsymbol{\nu}^{(*)} = (v_i^{(*)})_{i=1}^n$ ,  $\mathbf{f}^{(*)} = (f(\mathbf{x}_i^{(*)}))_{i=1}^n$  and  $\boldsymbol{\Theta} = \{\boldsymbol{\nu}, m^{(*)}, \theta^{(*)}, \sigma^2\}$ , the JGP model may be summarized as follows:

$$\begin{aligned} p(\mathbf{y}_n | \mathbf{f}^{(*)}, \boldsymbol{\nu}^{(*)}, \boldsymbol{\Theta}) &= \prod_{i=1}^n \mathcal{N}_1(y_i^{(*)} | f_i^{(*)}, \sigma^2)^{v_i^{(*)}} u^{1-v_i^{(*)}}, \\ p(\boldsymbol{\nu}^{(*)} | \boldsymbol{\nu}) &= \prod_{i=1}^n \pi(h(\mathbf{x}_i^{(*)}, \boldsymbol{\omega}))^{v_i^{(*)}} (1 - \pi(h(\mathbf{x}_i^{(*)}, \boldsymbol{\nu})))^{1-v_i^{(*)}}, \\ p(\mathbf{f}^{(*)} | m^{(*)}, \theta^{(*)}) &= \mathcal{N}_n(\mathbf{f}^{(*)} | m^{(*)} \mathbf{1}_n, \mathbf{C}_n), \end{aligned}$$

where  $\mathbf{y}_n = (y_i^{(*)})_{i=1}^n$  and  $\mathbf{C}_n$  is a  $n \times n$  matrix with  $c(x_i^{(*)}, x_j^{(*)}; \theta^{(*)})$  as its  $(i, j)$ th element. Parameters and latent indicators are learned via an EM-style algorithm, e.g., a variational EM variant (JGP-VEM) approximates the joint posterior over  $\{\boldsymbol{\nu}^{(*)}, \mathbf{f}^{(*)}\}$ , yielding similar predictive equations with uncertainty propagation.

Let  $\hat{v}_i^{(*)}$  represent the MAP estimate of  $v_i^{(*)}$  at the EM convergence and let  $\hat{\mathcal{D}}_n^{(*)} = \{i : \hat{v}_i^{(*)} = 1\}$  denote the estimated in-regime subset and  $\hat{\mathcal{D}}_o^{(*)} = \{1, \dots, n\} \setminus \hat{\mathcal{D}}_n^{(*)}$  the out-of-regime subset. Let

$\mathbf{y}_* = (y_i^{(*)}, i \in \hat{\mathcal{D}}_n^{(*)})$  and  $n_*$  denote the number of the elements in  $\hat{\mathcal{D}}_n^{(*)}$ . The posterior predictive mean and variance for  $f(\mathbf{x}_*)$  are

$$\begin{aligned}\mu_* &= \hat{m}^{(*)} + \mathbf{c}_{n_*}^\top (\hat{\sigma}^2 \mathbf{I}_{n_*} + \mathbf{C}_n^{(*)})^{-1} (\mathbf{y}_* - m^{(*)} \mathbf{1}), \\ \sigma_*^2 &= c(\mathbf{x}^{(*)}, \mathbf{x}^{(*)}; \hat{\theta}^{(*)}) - \mathbf{c}_{n_*}^\top (\hat{\sigma}^2 \mathbf{I}_{n_*} + \mathbf{C}_n^{(*)})^{-1} \mathbf{c}_{n_*},\end{aligned}\quad (3)$$

where  $\mathbf{c}_{n_*} = (c(\mathbf{x}_i^{(*)}, \mathbf{x}^{(*)}; \hat{\theta}_*^{(*)}))_{i \in \hat{\mathcal{D}}_n^{(*)}}$  is a column vector of the covariance values between  $\mathbf{y}_*$  and  $f(\mathbf{x}_*)$ , and  $\mathbf{C}_n^{(*)} = (c(\mathbf{x}_i^{(*)}, \mathbf{x}_j^{(*)}; \hat{\theta}_*^{(*)}))_{i, j \in \hat{\mathcal{D}}_n^{(*)}}$  is a square matrix of covariances evaluated for all pairs of  $\mathbf{y}_*$ . Here,  $\hat{\sigma}^2$ ,  $\hat{\theta}^{(*)}$  and  $\hat{m}^{(*)}$  represent the MLEs of  $\sigma^2$ ,  $\theta^{(*)}$  and  $m^{(*)}$  respectively.

When the input dimension  $D$  is large, several challenges arise for JGP modeling. First, the number of hyperparameters grows quickly: a linear partition function  $h(\mathbf{x}; \boldsymbol{\nu})$  requires  $D + 1$  parameters, while a quadratic function demands on the order of  $D^2 + 1$  parameters, quickly overwhelming the modest size of local neighborhoods. Second, there is a fundamental trade-off between bias and variance: enlarging the neighborhood yields more data for stable estimation of  $\boldsymbol{\nu}$ , but weakens the fidelity of the local Taylor approximation to complex boundaries; conversely, restricting to a small neighborhood preserves locality but risks overfitting due to limited data. Finally, the curse of dimensionality leads to sparse coverage in high-dimensional spaces, making it difficult to learn reliable regime boundaries without prior dimension reduction. These limitations motivate a unified framework that integrates dimensionality reduction directly into the JGP model, thereby enabling more effective modeling of high-dimensional, piecewise continuous functions.

### 2.3 Mahalanobis Gaussian Processes

Mahalanobis Gaussian Processes (AUEB et al., 2013) extend traditional Gaussian process models by incorporating a built-in dimensionality reduction. The input vector  $\mathbf{x}$  is linearly projected to  $\mathbf{W}\mathbf{x}$  by a linear projection matrix  $\mathbf{W} \in \mathbb{R}^{K \times D}$ . The relation of the projected features to the response is modeled as a stationary GP model with the covariance kernel defined on the projected features. For instance, the squared exponential covariance (1) can be defined with the projected features as

$$K_{\mathbf{W}}(\mathbf{x}_i, \mathbf{x}_j; \theta) = \sigma_f^2 \exp\left(-\frac{1}{2}(\mathbf{x}_i - \mathbf{x}_j)^\top \mathbf{W}^\top \mathbf{W}(\mathbf{x}_i - \mathbf{x}_j)\right). \quad (4)$$

To enable tractable learning, the authors introduced a variational inference framework for jointly estimating  $\mathbf{W}$  along with the remaining GP hyperparameters.

Deep Variational Mahalanobis Gaussian Processes (DMGPs) (de Souza et al., 2022) extend MGPs by introducing a nonlinear, input-dependent projection. Unlike MGPs, which employ a single global linear projection  $\mathbf{W}$ , DMGP assigns each data point  $\mathbf{x}$  its own projection matrix  $\mathbf{W}(\mathbf{x})$ . This results in a non-linear projection  $g(\mathbf{x}) = \mathbf{W}(\mathbf{x})\mathbf{x}$ . Each entry of  $\mathbf{W}(\mathbf{x})$  is modeled as a function of  $\mathbf{x}$ , governed by a stationary GP. Within each row of  $\mathbf{W}(\mathbf{x})$ , the elements share a common GP prior with identical kernel hyperparameters. This construction enforces equal scaling of elements within a row through the shared kernel variance parameter, thereby achieving automatic relevance determination for the associated latent dimension.

DMGP assigns a distinct linear projection  $\mathbf{W}(\mathbf{x})$  to each input location  $\mathbf{x}$ . However, this pointwise projection does not form a feasible combination with local models such as JGP, because the large number of the linear projection matrices easily makes an overfit to a small amount of local training data  $\mathcal{D}_n(\mathbf{x}_*)$  in JGP. This motivates our main contribution, which integrates local projection into

JGP under a variational framework. In the newly proposed DJGP, we seek for a locally constant approximation of  $\mathbf{W}(\mathbf{x})$ . When  $\mathbf{W}(\mathbf{x})$  is a smooth function of  $\mathbf{x}$ , the local constant approximation can be justified by the zero-order Taylor approximation. Specifically,  $\mathbf{W}(\mathbf{x})$  is approximately equal to  $\mathbf{W}(\mathbf{x}_*)$  for the local data  $\mathcal{D}_n(\mathbf{x}_*)$  nearby a test location  $\mathbf{x}_*$ . Under this formulation, the JGP model for  $\mathbf{x}_*$  requires only a single projection matrix in addition to its standard parameters. This substantially reduces the number of parameters to estimate, improving feasibility while still capturing nonlinear projections through a piecewise constant structure.

### 3. Deep Jump Gaussian Process (DJGP)

Let  $\mathcal{X}$  denote a domain of a function in  $\mathbb{R}^D$ . We consider a problem of estimating an unknown surrogate function which relates inputs  $\mathbf{x} \in \mathcal{X}$  to a real response variable. We assume the existence of a nonlinear sufficient dimension reduction (for the unknown surrogate relation), which reduces the  $D$ -dimensional feature in  $\mathcal{X}$  to a lower-dimensional feature in  $\mathcal{Z} \subseteq \mathbb{R}^K$  via a continuously differentiable mapping,

$$g : \mathcal{X} \longrightarrow \mathcal{Z} \subseteq \mathbb{R}^K, \quad K \ll D,$$

so that the response variable depends on  $\mathbf{x}$  only through its reduced representation  $\mathbf{z} = g(\mathbf{x})$ . Therefore, we can introduce a reduced surrogate model  $f$  to relate  $\mathbf{z}$  to the response variable. We assume  $f$  is assumed to be piecewise continuous in  $\mathbf{z}$ , so the composition function  $f \circ g$  is also piecewise continuous in  $\mathbf{x}$ , given the assumed continuity of  $g$ . Specifically, there exists an (unknown) integer  $M$  and an unknown partition of  $\mathcal{Z}$  into disjoint regions  $\{\mathcal{Z}_k\}_{k=1}^M$  such that

$$f(\mathbf{z}) = \sum_{m=1}^M f_k(\mathbf{z}) 1_{\mathcal{Z}_m}(\mathbf{z}), \quad (5)$$

where each local function  $f_k$  is a continuous function with its uncertainty modeled as a stationary Gaussian process (GP) with constant mean  $\mu_m \in \mathbb{R}$  and a stationary covariance function  $c_m(\cdot, \cdot)$ . We assume mutual independence across regions:

$$\text{Independence:} \quad f_m \text{ is independent of } f_\ell \text{ for } m \neq \ell. \quad (6)$$

which implies zero correlation between function values belonging to different regions.

For simplifying the model exposition, we restrict  $c_m$  to a parametric family  $c(\cdot, \cdot; \theta) : \theta \in \Theta$ , though the framework extends naturally to more general covariance functions. Let  $\theta_m \in \Theta$  denote the region-specific covariance parameter so that  $c_m(\cdot, \cdot) = c(\cdot, \cdot; \theta_m)$ . We specifically consider the scale family,

$$c(\mathbf{z}, \mathbf{z}'; \theta_m) = a_m C(b_m \|\mathbf{z} - \mathbf{z}'\|_2),$$

where  $\|\mathbf{z} - \mathbf{z}'\|_2$  is the Euclidean distance,  $C(\cdot)$  is an isotropic correlation function with a unit length scale,  $a_m > 0$  is the variance parameter, and  $b_m > 0$  is the length scale parameter.

Finally, we assume heterogeneity in region means:

$$\text{Heterogeneity:} \quad \mu_m \neq \mu_\ell, \theta_m \neq \theta_\ell \quad \text{for every pair of } m \neq \ell. \quad (7)$$

We aim to predict the surrogate response  $f \circ g(\mathbf{x})$  at  $J$  test locations  $\{\mathbf{x}^{(j)} \in \mathcal{X}, j = 1, \dots, J\}$ , given  $N$  noisy observations from the underlying model. Each observation at  $\mathbf{x}_i$  is given as

$$y_i = f(g(\mathbf{x}_i)) + \epsilon_i, \quad i = 1, \dots, N, \quad (8)$$

where the noise terms are independent, with  $\epsilon_i \sim \mathcal{N}(0, \sigma^2(g(\mathbf{x}_i)))$ . The noise variance is assumed to change smoothly in the projected input  $g(\mathbf{x}_i)$  and thus also smooth in the original input  $\mathbf{x}_i$ , so the variance is approximately constant around a small neighborhood of the projected input  $g(\mathbf{x}_i)$ .

### 3.1 Local Approximation

Modeling and estimating the complex functions  $g$  and  $f$  explicitly together with the unknown partition  $\{\mathcal{Z}_m\}_{m=1}^M$  is challenging. Following the JGP framework, we instead seek a local approximation. For each test location  $\mathbf{x}_*^{(j)}$ , we first select a small subset of nearby training data—for example, the  $n$  nearest neighbors of  $\mathbf{x}_*^{(j)}$  or a subset chosen by an existing local selection criterion (Gramacy and Apley, 2015). We denote this local dataset by

$$\mathcal{D}_n^{(j)} = \{(\mathbf{x}_i^{(j)}, y_i^{(j)}) : i = 1, \dots, n\} = (\mathbf{X}^{(j)}, \mathbf{y}^{(j)}), \quad (9)$$

where  $\mathbf{x}_i^{(j)}$  and  $y_i^{(j)}$  represent the input vector and corresponding response of the  $i$ th local data.

Since we assumed the map  $g$  is smooth (at least continuously differentiable), we can take the first-order Taylor approximation to  $g$  around a small neighborhood of  $\mathbf{x}_*^{(j)}$ . Therefore, for each local data  $(\mathbf{x}_i^{(j)}, y_i^{(j)})$ ,

$$g(\mathbf{x}_i^{(j)}) \approx g(\mathbf{x}_*^{(j)}) + \mathbf{W}_j(\mathbf{x}_i^{(j)} - \mathbf{x}_*^{(j)}). \quad (10)$$

The constant terms in the approximation do not affect the downstream GP modeling. Therefore, we omit the constant terms and define a local projection by  $g(\mathbf{x}_i^{(j)}) \approx \mathbf{W}_j \mathbf{x}_i^{(j)}$  for the local data.

The projection matrix  $\mathbf{W}_j$  defines the direction of the local projection. To impose statistical correlation and encourage smooth variation of the projections over  $\mathcal{X}$ , we place a stationary Gaussian process prior on the collection of local projection matrices  $\mathbf{W} = \{\mathbf{W}_j\}_{j=1}^J$ . Specifically, let  $w_{kd}^{(j)}$  denote the  $(k, d)$ -th entry of  $\mathbf{W}_j$ , and define the vector  $\mathbf{w}_{kd} = [w_{kd}^{(1)}, \dots, w_{kd}^{(J)}]$ , which includes the  $(k, d)$ th entries across all local projection matrices. We then model  $\mathbf{w}_{kd}$  as a Gaussian process with zero mean and the isotropic covariance function given by

$$c_{iso}(\mathbf{x}_*^{(j)}, \mathbf{x}_*^{(j')}; s, \ell_{w,k}) = s^2 \exp\left(-\frac{\|\mathbf{x}_*^{(j)} - \mathbf{x}_*^{(j')}\|^2}{2\ell_{w,k}^2}\right).$$

The square exponential covariance function models the correlation between two local project matrices,  $\mathbf{W}_j$  and  $\mathbf{W}_{j'}$ , as a function of the square distance between the corresponding test locations  $\mathbf{x}_*^{(j)}$  and  $\mathbf{x}_*^{(j')}$ . All entries of the projection matrices share a common variance parameter  $s^2$ , while elements within each row additionally share a row-specific length-scale parameter  $\ell_{w,k}$ . This design enforces equal scaling of elements within a row, enabling automatic relevance determination for the corresponding latent dimension. Accordingly, the joint prior would be

$$p(\mathbf{W} | \Theta_{\mathbf{W}}) = \prod_{k=1}^K \prod_{d=1}^D \mathcal{N}(\mathbf{w}_{kd} | \mathbf{0}_J, \mathbf{C}_w^{(k)}), \quad (11)$$

where  $\mathbf{0}_J$  is a  $J$ -dimensional column vector of zeros, and  $\mathbf{C}_w^{(k)}$  is a  $J \times J$  matrix with  $c_{iso}(\mathbf{x}_*^{(j)}, \mathbf{x}_*^{(j')}; s, \ell_{w,k})$  as its  $(j, j')$  entry, and  $\Theta_{\mathbf{W}} = (s, \ell_{w,1}, \dots, \ell_{w,K})$ .

Conditioned on the local projection  $\mathbf{W}_j$ , the projected local dataset is defined as

$$\mathcal{D}_{\mathbf{W}_j, n}^{(j)} = \{(\mathbf{z}_i^{(j)}, y_i^{(j)}) : i = 1, \dots, n, \mathbf{z}_i^{(j)} = \mathbf{W}_j \mathbf{x}_i^{(j)}\}. \quad (12)$$

By the mixture proposition in (5), these local data may originate from different regions, in which case the input–response relationship cannot be captured by a single Gaussian process. We follow JGP to model the mixture data. Specifically, in the  $j$ th local region, we introduce binary latent variables  $v_i^{(j)} \in \{0, 1\}$ , to indicate that the projected training input  $\mathbf{z}_i^{(j)}$  belongs to the same region as the projected test point  $\mathbf{W}_j \mathbf{x}_*^{(j)}$  ( $v_i^{(j)} = 1$ ) or not ( $v_i^{(j)} = 0$ ). Based on the indicator values, the local data  $\mathcal{D}_{\mathbf{W}_j, n}^{(j)}$  can be partitioned into two groups:  $\mathcal{D}_{\mathbf{W}_j, n}^{(j,1)} = \{i \in \{1, \dots, n\} : v_i^{(j)} = 1\}$  and the remainder  $\mathcal{D}_{\mathbf{W}_j, n}^{(j,0)} = \{1, \dots, n\} \setminus \mathcal{D}_{\mathbf{W}_j, n}^{(j,1)}$ . The first group belongs to the same region as the projected test location  $\mathbf{W}_j \mathbf{x}_*^{(j)}$ , so we use them to predict  $f$  at the test location. The second group is independent of  $f$ , based on the independence assumption (6), so it would be not used.

Since we are uncertain about the indicator values, we model them as random variables. We assign the prior probability to the indicator variables as in the JGP model (2),

$$p(v_i^{(j)} = 1 | \mathbf{v}_j) = \pi(h(\mathbf{z}_i^{(j)}; \mathbf{v}_j)),$$

where  $\pi(z) = 1/(1 + e^{-z})$  is the sigmoid link function, and we use the linear decision function  $h(\mathbf{z}_i^{(j)}; \mathbf{v}_j) = \mathbf{v}_j^T [1, \mathbf{z}_i^{(j)}]$ . The logistic model divides the local data by the linear boundary,  $\mathbf{v}_j^T [1, \mathbf{z}_i^{(j)}] = 0$ . When the boundaries of the regions  $\{\mathcal{Z}_m, m = 1, \dots, M\}$  are smooth enough, the boundaries can be locally linearly approximated according to the Taylor approximation, so the use of the linear boundary to split the local data is justifiable. When the boundaries are expected more rough, one can use higher order models such as quadratic or higher order polynomial functions.

The first group of the local data  $\{(\mathbf{z}_i^{(j)}, y_i^{(j)}) : v_i^{(j)} = 1\}$  and the projected test point  $\mathbf{W}_j \mathbf{x}_*^{(j)}$  belongs to the same region, denoted  $m(j)$ . Based on the model assumption (5), the input-output relation follows a stationary Gaussian process with the constant mean  $\mu_{m(j)}$  and the covariance function  $c(\cdot, \cdot; \theta_{m(j)})$ . The region-specific covariance function is in the form of

$$c(\mathbf{z}, \mathbf{z}'; \theta_{m(j)}) = a_{m(j)} C(b_{m(j)} \|\mathbf{z} - \mathbf{z}'\|_2).$$

Since the local length scale parameter is redundant to the scale of the local projection matrix  $\mathbf{W}_j$ , we remove the length scale parameter. The removal makes the regional covariance function to have only the scale parameter  $a_{m(j)}$  as

$$c(\mathbf{z}, \mathbf{z}'; a_{m(j)}) = a_{m(j)} C(\|\mathbf{z} - \mathbf{z}'\|_2).$$

Based on (8),  $y_i$  is a noisy realization of the Gaussian process

$$p(y_i^{(j)} | f_i^{(j)}, v_i^{(j)} = 1, \sigma_j^2) = \mathcal{N}(y_i^{(j)} | f_i^{(j)}, \sigma_j^2), \quad (13)$$

where  $\sigma_j^2$  is a local constant approximation to  $\sigma^2(g(\mathbf{x}))$  at  $\mathbf{x}$  around  $\mathbf{x}_*^{(j)}$ . The Taylor approximation is justifiable given smoothness of  $\sigma^2(\cdot)$  and  $g(\cdot)$ .

The other group of the local data  $\{(\mathbf{z}_i^{(j)}, y_i^{(j)}) : v_i^{(j)} = 0\}$  is independent of the response variable at the projected test point  $\mathbf{W}_j \mathbf{x}_*^{(j)}$ . We treat them as outliers with respect to  $f^{(j)}$  and assign them a uniform likelihood,

$$p(y_i^{(j)} | v_i^{(j)} = 0) = \frac{1}{u_j}. \quad (14)$$

Pulling all local data, latent variables and hyperparameters together, let  $\mathbf{y}^{(j)} = (y_1^{(j)}, \dots, y_n^{(j)})$ ,  $\mathbf{v}^{(j)} = (v_1^{(j)}, \dots, v_n^{(j)})$ ,  $\mathbf{f}^{(j)} = (f_1^{(j)}, \dots, f_n^{(j)})$  and  $\Theta^{(j)} = (\mathbf{v}_j, \sigma_j^2, \mu_{m(j)}, a_{m(j)})$ . The conditional distribution is therefore

$$p(\mathbf{y}^{(j)} | \mathbf{v}^{(j)}, \mathbf{f}^{(j)}, \Theta^{(j)}) = \prod_{i=1}^n \left[ \mathcal{N}(y_i^{(j)} | f_i^{(j)}, \sigma_j^2) \right]^{v_i^{(j)}} \left[ \frac{1}{u_j} \right]^{1-v_i^{(j)}}, \text{ and}$$

$$p(\mathbf{v}^{(j)} | \Theta^{(j)}) = \prod_{i=1}^n \left[ p(v_i^{(j)} = 1 | \mathbf{v}_j) \right]^{v_i^{(j)}} \left[ 1 - p(v_i^{(j)} = 1 | \mathbf{v}_j) \right]^{1-v_i^{(j)}}.$$

The joint distribution for the local model is

$$p(\mathbf{y}^{(j)}, \mathbf{v}^{(j)}, \mathbf{f}^{(j)} | \mathbf{W}_j, \Theta^{(j)}) = p(\mathbf{y}^{(j)} | \mathbf{v}^{(j)}, \mathbf{f}^{(j)}, \Theta^{(j)}) \times p(\mathbf{v}^{(j)} | \Theta^{(j)}) \times p(\mathbf{f}^{(j)} | \mathbf{W}_j, \Theta^{(j)}),$$

where  $p(\mathbf{f}^{(j)} | \mathbf{W}_j, \Theta^{(j)}) = \mathcal{N}(\mathbf{f}^{(j)} | \mu_{m(j)} \mathbf{1}_n, a_{m(j)} \mathbf{C}_{nn})$ , and  $\mathbf{C}_{nn}$  is a  $n \times n$  matrix with  $C(\|\mathbf{z}_i^{(j)} - \mathbf{z}_{i'}^{(j)}\|_2)$  as its  $(i, i')$ th element.

The full joint distribution is

$$p(\mathbf{y}, \mathbf{v}, \mathbf{f}, \mathbf{W} | \Theta) = p(\mathbf{W} | \Theta_{\mathbf{W}}) \times \prod_{j=1}^J p(\mathbf{y}^{(j)}, \mathbf{v}^{(j)}, \mathbf{f}^{(j)} | \mathbf{W}_j, \Theta^{(j)}), \quad (15)$$

where  $\mathbf{y} = (\mathbf{y}^{(1)}, \dots, \mathbf{y}^{(J)})$ ,  $\mathbf{v} = (\mathbf{v}^{(1)}, \dots, \mathbf{v}^{(J)})$ ,  $\mathbf{f} = (\mathbf{f}^{(1)}, \dots, \mathbf{f}^{(J)})$ , and  $\Theta = (\Theta_{\mathbf{W}}, \Theta^{(1)}, \dots, \Theta^{(J)})$ . Conditioned on the local projection matrix  $\mathbf{W}_j$ , the conditional model  $p(\mathbf{y}^{(j)}, \mathbf{v}^{(j)}, \mathbf{f}^{(j)} | \mathbf{W}_j, \Theta^{(j)})$  is a local model, a JGP model specific to the local projection data  $\mathcal{D}_{\mathbf{W}_j, n}^{(j)}$ . The local project matrices are correlated through the global GP model  $p(\mathbf{W})$ . This unique two-layer GP/JGP model is referred to as the Deep JGP (DJGP) model.

### 3.2 Variational Inference

The statistical inference of the model parameters  $\Theta$  and the latent variables  $\mathbf{f}$ ,  $\mathbf{W}$ , and  $\mathbf{v}$  is analytically intractable due to the nonlinear dependencies introduced by the hierarchical structure. To address this challenge, we adopt a variational inference framework, following the sparse GP methodology introduced in MGP (AUEB et al., 2013) and DMGP (de Souza et al., 2022). Specifically, we introduce two sets of inducing variables: local inducing variables for the latent functions  $\mathbf{f}$  to decouple the otherwise intractable dependencies between latent variables and hyperparameters, and global inducing variables for the projection process  $\mathbf{W}$  to alleviate the prohibitive computational burden associated with repeated large-scale matrix inversions, when the number of the test locations is large.

**Local inducing variables.** For each local region associated with a test point  $\mathbf{x}_*^{(j)}$ , we introduce  $L_1$  local inducing inputs

$$\tilde{\mathbf{z}}_\ell^{(j)} \in \mathbb{R}^K, \quad \ell = 1, \dots, L_1,$$

with corresponding inducing outputs  $r_\ell^{(j)}$ . These outputs are defined as standardized evaluations of the latent function  $f_{m(j)}$ ,

$$r_\ell^{(j)} = \frac{f_{m(j)}(\tilde{\mathbf{z}}_\ell^{(j)}) - \mu_{m(j)}}{a_{m(j)}},$$

so that they are independent of the amplitude and mean hyperparameters  $a_{m(j)}$  and  $\mu_{m(j)}$ , which improves identifiability. Collecting them as  $\mathbf{r}^{(j)} = (r_\ell^{(j)})_{\ell=1}^{L_1} \in \mathbb{R}^{L_1}$ , we assume the joint Gaussian prior

$$p(\mathbf{r}^{(j)}) = \mathcal{N}(\mathbf{r}^{(j)} \mid \mathbf{0}_{L_1}, \mathbf{K}_r^{(j)}),$$

where  $\mathbf{K}_r^{(j)} \in \mathbb{R}^{L_1 \times L_1}$  has entries  $[\mathbf{K}_r^{(j)}]_{\ell\ell'} = C\left(\|\tilde{\mathbf{z}}_\ell^{(j)} - \tilde{\mathbf{z}}_{\ell'}^{(j)}\|\right)$ . Conditioned on these inducing variables, the local latent function values  $\mathbf{f}^{(j)}$  follow

$$p(\mathbf{f}^{(j)} \mid \mathbf{r}^{(j)}, \mathbf{W}_j, \Theta^{(j)}) = \mathcal{N}\left(\mathbf{f}^{(j)} \mid \mathbf{K}_{fr}^{(j)} (\mathbf{K}_r^{(j)})^{-1} \mathbf{r}^{(j)}, a_{m(j)} \mathbf{C}_{nn} - \mathbf{K}_{fr}^{(j)} (\mathbf{K}_r^{(j)})^{-1} (\mathbf{K}_{fr}^{(j)})^\top\right),$$

where  $\mathbf{K}_{fr}^{(j)} \in \mathbb{R}^{n \times L_1}$  with entries  $[\mathbf{K}_{fr}^{(j)}]_{i\ell} = a_{m(j)} C(\|\mathbf{W}_j \mathbf{x}_i^{(j)} - \tilde{\mathbf{z}}_\ell^{(j)}\|^2)$ , and  $\mathbf{C}_{nn}$  denotes the kernel matrix constructed over the projected local inputs.

**Global inducing variables.** Similarly, for the projection process, we introduce  $L_2$  global inducing inputs

$$\tilde{\mathbf{x}}_\ell \in \mathbb{R}^D, \quad \ell = 1, \dots, L_2,$$

with inducing outputs  $\mathbf{R}_\ell \in \mathbb{R}^{K \times D}$ , aggregated as  $\mathbf{R} = (\mathbf{R}_\ell)_{\ell=1}^{L_2} \in \mathbb{R}^{L_2 \times K \times D}$ . The inducing outputs are assumed to be drawn from the same GP as  $\mathbf{W}_j$ . Specifically, let  $r_{kd}^{(\ell)}$  denote the  $(k, d)$ -th entry of  $\mathbf{R}_\ell$ , and define the vector  $\mathbf{r}_{kd} = [r_{kd}^{(1)}, \dots, r_{kd}^{(L_2)}]$ , which includes the  $(k, d)$ th entries across all inducing output matrices. Then,  $\mathbf{r}_{kd}$  is assumed to follow the same stationary GP as  $\omega_{kd}$ . The prior distribution of  $\mathbf{R}$  is given as

$$p(\mathbf{R} \mid \Theta_W) = \prod_{k=1}^K \prod_{d=1}^D \mathcal{N}(\mathbf{r}_{kd} \mid \mathbf{0}_{L_2}, \mathbf{K}_R^{(k)}), \quad (16)$$

where  $\mathbf{K}_R^{(k)}$  is a  $L_2 \times L_2$  matrix with its  $(\ell, \ell')$ th entry as  $c_{iso}(\tilde{\mathbf{x}}_\ell, \tilde{\mathbf{x}}_{\ell'}; s, \ell_{w,k})$ . To reduce the computational burden when the number of test points  $J$  is large, we use the sparse Gaussian process approximation. It assumes that the conditional independence of the elements in  $\mathbf{w}_{k,d}$  conditioned on  $\mathbf{r}_{kd}$ , which would give the conditional distribution as

$$p(\mathbf{W} \mid \mathbf{R}, \Theta_W) = \prod_{k=1}^K \prod_{d=1}^D \mathcal{N}\left(\mathbf{w}_{kd} \mid \mathbf{K}_{WR}^{(k)} (\mathbf{K}_R^{(k)})^{-1} \mathbf{r}_{kd}, \Lambda_W^{(k)} - \mathbf{K}_{WR}^{(k)} (\mathbf{K}_R^{(k)})^{-1} \mathbf{K}_{WR}^{(k)\top}\right).$$

where  $\Lambda_W^{(k)}$  is a  $J \times J$  diagonal matrix with its  $j$ th diagonal element equal to  $c_{iso}(\mathbf{x}_*^{(j)}, \mathbf{x}_*^{(j)}; s, \ell_{w,k})$ ,  $\mathbf{K}_{WR}^{(k)}$  is a  $J \times L_2$  matrix with its  $(j, \ell)$ th element equal to  $c_{iso}(\mathbf{x}_*^{(j)}, \tilde{\mathbf{x}}_\ell; s, \ell_{w,k})$ .

**Variational family and ELBO.** The full posterior distribution with the two sets of the inducing variables is

$$\begin{aligned} p(\mathbf{v}, \mathbf{f}, \mathbf{W}, \mathbf{R}, \mathbf{r} \mid \mathbf{y}, \Theta) \\ \propto p(\mathbf{W} \mid \mathbf{R}, \Theta_W) \times p(\mathbf{R} \mid \Theta_W) \\ \times \prod_{j=1}^J p(\mathbf{y}^{(j)} \mid \mathbf{v}^{(j)}, \mathbf{f}^{(j)}, \Theta^{(j)}) \times p(\mathbf{v}^{(j)} \mid \Theta^{(j)}, \mathbf{W}_j) \times p(\mathbf{f}^{(j)} \mid \mathbf{r}^{(j)}, \mathbf{W}_j, \Theta^{(j)}) \times p(\mathbf{r}^{(j)}) \end{aligned} \quad (17)$$

We approximate it with the following factorized variational distribution:

$$q(\mathbf{v}, \mathbf{f}, \mathbf{W}, \mathbf{R}, \mathbf{r}) = p(\mathbf{W} | \mathbf{R}, \Theta_{\mathbf{W}}) \times q(\mathbf{R}) \times \prod_{j=1}^J \left[ q(\mathbf{v}^{(j)}) p(\mathbf{f}^{(j)} | \mathbf{r}^{(j)}, \mathbf{W}_j, \Theta^{(j)}) q(\mathbf{r}^{(j)}) \right].$$

with

$$\begin{aligned} q(\mathbf{v}^{(j)}) &= \prod_{i \in \mathcal{D}_n^{(j)}} q(v_i^{(j)}) \text{ with } q(v_i^{(j)}) = \text{Bernoulli}(\rho_i^{(j)}) \\ q(\mathbf{r}^{(j)}) &= \mathcal{N}(\boldsymbol{\mu}_r^{(j)}, \boldsymbol{\Sigma}_r^{(j)}), \\ q(\mathbf{R}) &= \prod_{\ell=1}^{L_2} \prod_{k=1}^K \prod_{d=1}^D q(r_{kd}^{(\ell)}) \text{ with } q(r_{kd}^{(\ell)}) = \mathcal{N}(\mu_{lkd}, \sigma_{lkd}^2). \end{aligned}$$

The distribution parameters,  $\rho_i^{(j)}$ ,  $\boldsymbol{\mu}_r^{(j)}$ ,  $\boldsymbol{\Sigma}_r^{(j)}$ ,  $\mu_{lkd}$  and  $\sigma_{lkd}$ , are unknown, variational parameters to optimize. We denote them collectively by  $\Theta_{\mathbf{V}}$ .

Under this, the evidence lower bound (ELBO) decomposes as

$$\begin{aligned} \mathcal{L} &= \sum_{j=1}^J \left\{ \mathbb{E}_{q(\mathbf{r}^{(j)})q(\mathbf{W}_j)q(\mathbf{v}^{(j)})} [\log p(\mathbf{y}^{(j)} | \mathbf{v}^{(j)}, \mathbf{f}^{(j)}, \Theta^{(j)})] \right. \\ &\quad \left. + \mathbb{E}_{q(\mathbf{W}_j)q(\mathbf{v}^{(j)})} [\log p(\mathbf{v}^{(j)} | \Theta^{(j)}, \mathbf{W}_j) - \log q(\mathbf{v}^{(j)})] - \text{KL}(q(\mathbf{r}^{(j)}) \parallel p(\mathbf{r}^{(j)})) \right\} \\ &\quad - \text{KL}(q(\mathbf{R}) \parallel p(\mathbf{R} | \Theta_{\mathbf{W}})), \end{aligned} \tag{18}$$

where  $q(\mathbf{W}_j) = \mathbb{E}_{q(\mathbf{R})} [p(\mathbf{W}_j | \mathbf{R})]$ . The detailed derivation of the ELBO is provided in Appendix A.

In practice, we maximize  $\mathcal{L}$  by stochastic gradient ascent with respect to the variational parameters  $\Theta_{\mathbf{V}}$ , the inducing inputs  $\tilde{\mathbf{x}} = (\tilde{\mathbf{x}}_{\ell})_{\ell=1}^{L_2}$ , and the model hyperparameters  $\Theta$ . We fixed the local inducing inputs  $\{\tilde{\mathbf{z}}_{\ell}^{(j)}\}_{\ell=1}^{L_1}$  to randomly sampled values, specifically,  $\tilde{\mathbf{z}}_{\ell}^{(j)} \sim \mathcal{N}(\mathbf{0}, \mathbf{I}_Q)$ , because the learning output was not very sensitive to the choices. In contrast, the global inducing inputs  $\{\tilde{\mathbf{x}}_{\ell}\}_{\ell=1}^{L_2}$  are treated as learnable parameters and jointly optimized with the other model parameters.

To encourage a reasonable initialization before optimization, we draw them around the empirical mean of the training inputs with random perturbations proportional to the empirical standard deviation, that is,  $\tilde{\mathbf{x}}_{\ell} = \bar{\mathbf{x}} + \boldsymbol{\epsilon}_{\ell} \odot \boldsymbol{\sigma}_x$  with  $\boldsymbol{\epsilon}_{\ell} \sim \mathcal{N}(\mathbf{0}, \mathbf{I}_D)$ , where  $\bar{\mathbf{x}}$  and  $\boldsymbol{\sigma}_x$  denote the element-wise mean and standard deviation of the training data. This scheme ensures that the global inducing points are well spread within the data manifold and provides a stable starting point for subsequent variational optimization.

Following (AUEB et al., 2013), the global kernel hyperparameters and inducing inputs are optimized via a Type-II maximum likelihood (empirical Bayes) approach, which has been shown to yield robust and computationally efficient performance for Mahalanobis-type Gaussian process models.

### 3.3 Prediction

To mitigate any suboptimality of the variational approximation, we use a two-stage, sampling-based prediction. We follow the approach of (AUEB et al., 2013) (2013, Sec. 2.5, Eqs. (17)–(18)) and adapt it to our model. For each test location, we takes a random sample of the projection matrices drawn from its estimated variational posterior distribution  $q(\mathbf{W}_j)$ . Each sampled projection defines a

different low-dimensional embedding, and the predictive mean and variance are obtained by averaging the corresponding GP predictions. Sampling from  $q(\mathbf{W}_j)$  provides a computationally efficient and statistically robust way to propagate the uncertainty of the learned projection into the Jump GP predictions.

Specifically, for each test input  $\mathbf{x}^{(j)}$ , we first draw  $M_c$  samples

$$\mathbf{W}_j^{(m)} \sim q(\mathbf{W}_j), \quad m = 1, \dots, M_c,$$

from the variational posterior over the projection matrix. Each sample defines a low-dimensional embedding of the training data  $\mathbf{z}_i^{(j,m)} = \mathbf{W}_j^{(m)} \mathbf{x}_i^{(j)}$  for  $i = 1, \dots, n$ . Let  $\mathbf{Z}^{(i,m)}$  denote the  $n$  locally embedded training inputs. We then fit a standard Jump GP on  $(\mathbf{Z}^{(i,m)}, \mathbf{y}^{(j)})$  to obtain the predictive mean  $\mu_*^{(j,m)}$  and variance  $\sigma_*^{2(j,m)}$ , according to the posterior expressions in Eq. (3) of Section 2.2. The final prediction for region  $j$  is computed by averaging over the  $M_c$  Monte Carlo samples. Finally, we aggregate via Monte Carlo:

$$\mu_*^{(j)} = \frac{1}{M_c} \sum_{m=1}^{M_c} \mu_*^{(j,m)}, \quad \sigma_*^{2(j)} = \frac{1}{M_c} \sum_{m=1}^{M_c} \left[ \sigma_*^{2(j,m)} + (\mu_*^{(j,m)} - \mu_*^{(j)})^2 \right].$$

This procedure leverages the global consistency of the variational posterior for each  $\mathbf{W}_j$  while retaining the local adaptivity and uncertainty calibration of Jump GP in the learned subspace. The detailed pseudo-algorithm could be found in Algorithm 1.

#### 4. Synthetic Dataset Experiments

We assess the performance of DJGP on two simulated examples, comparing against several baseline methods. All methods are implemented in Python<sup>1</sup>. All experiments are conducted on a workstation equipped with a 13th Gen Intel(R) Core(TM) i7-13700 CPU (2.10 GHz), 32 GB of RAM, and multiple GPUs with a total of 4 GB graphics memory, running a 64-bit Windows 11 operating system. We report both root mean squared error (RMSE) and continuous ranked probability score (CRPS) as evaluation metrics; we favor CRPS over negative log predictive density (NLPD) because of NLPD’s sensitivity to outliers. When it compares a Gaussian predictive distribution  $\mathcal{N}(\mu_j, \sigma_j^2)$  at the  $j$ th test site ( $j = 1, \dots, J$ ) with the test response  $y_*^{(j)}$ , the two metrics are defined as

$$\text{RMSE} = \sqrt{\frac{1}{J} \sum_{j=1}^J (y_*^{(j)} - \mu_j)^2}, \quad (19)$$

$$\text{CRPS} = \frac{1}{J} \sum_{j=1}^J \text{CRPS}(\mathcal{N}(\mu_j, \sigma_j^2), y_*^{(j)}), \quad (20)$$

where the CRPS is defined by

$$\text{CRPS}(\mathcal{N}(\mu, \sigma^2), y) = \sigma \left[ z(2\Phi(z) - 1) + 2\phi(z) - \frac{1}{\sqrt{\pi}} \right], \quad z = \frac{y - \mu}{\sigma},$$

with  $\Phi(\cdot)$  and  $\phi(\cdot)$  the standard normal CDF and PDF, respectively.

1. The complete Python codebase—including scripts for benchmark models—is available at <https://github.com/crushonyfg/DJGP>.

---

**Algorithm 1** DJGP: Variational Training & Prediction

---

**Require:** Region data  $\{(\mathcal{D}_n^{(j)}, \mathbf{x}_*^{(j)})\}_{j=1}^J$ , initial values of the variational parameters  $\Theta_V$ , inducing inputs/outputs  $\{(\tilde{z}_\ell^{(j)}, r_\ell^{(j)}) : \ell = 1, \dots, L_1, j = 1, \dots, J\}$  and  $\{(\tilde{x}_\ell, \mathbf{R}_\ell) : \ell = 1, \dots, L_2\}$ , and other hyperparameters  $\Theta$ , learning rate  $\eta$ , max iterations  $S$ ,  $M_c$

**Ensure:** Posterior approximations and predictive distribution at test points

- 1: **for**  $s = 1$  to  $S$  **do**
- 2:   Compute  $\mathcal{L}$  and its gradients w.r.t. all variational and model parameters ()
- 3:   Update parameters by gradient ascent:  $\theta \leftarrow \theta + \eta \nabla_\theta \mathcal{L}$
- 4:   Enforce positivity constraints on variances and lengthscales
- 5:   **If** ELBO has converged **then break**
- 6: **end for**
- 7: **Prediction:**
- 8: **for** each test region  $j$  **do**
- 9:   Compute posterior  $q(\mathbf{W}_j)$  from  $q(\mathbf{R})$  and conditional GP prior
- 10:   Draw  $M_c$  samples  $\{\mathbf{W}_j^{(m)}\} \sim q(\mathbf{W}_j)$
- 11:   **for**  $m = 1$  to  $M_c$  **do**
- 12:     Project data:  $\tilde{\mathbf{Z}}^{(j)} = \mathbf{W}_j^{(m)} \mathbf{X}^{(j)}$ ,  $\tilde{\mathbf{z}}_*^{(j)} = \mathbf{W}_j^{(m)} \mathbf{x}_*^{(j)}$
- 13:     Fit local Jump GP on  $(\tilde{\mathbf{Z}}^{(j)}, \mathbf{y}^{(j)})$  to predict  $\mu_*^{(j,m)}, \sigma_*^{2(j,m)}$
- 14:   **end for**
- 15:   Aggregate  $\mu_*^{(j)} = \frac{1}{M_c} \sum_m \mu_*^{(j,m)}$ ,  $\sigma_*^{2(j)} = \frac{1}{M_c} \sum_m [\sigma_*^{2(j,m)} + (\mu_*^{(j,m)} - \mu_*^{(j)})^2]$
- 16: **end for**
- 17: **return**  $\{\mu_*^{(j)}, \sigma_*^{2(j)}\}_{j=1}^J$

---

**Baseline Methods** The first baseline is the original Jump Gaussian Process (**JGP**) proposed by Park et al. (Park, 2022), implemented with classification EM and linear partition boundaries. We restrict JGP to linear separators to avoid overfitting in high-dimensional settings and to ensure a fair comparison with DJGP, which also assumes linear boundaries but can be readily extended to quadratic ones. The second baseline is **JGP-SIR**, which applies sliced inverse regression (SIR) (Li, 1991) to reduce the input dimension before fitting a standard JGP on the projected features. The third baseline is **JGP-AE**, which employs an autoencoder for dimensionality reduction, followed by fitting JGP in the learned low-dimensional space. The autoencoder is implemented as a multi-layer perceptron (MLP) for both encoder and decoder. Fourth, we include a two-layer, doubly-stochastic Deep Gaussian Process (**DGP**) implemented using GPyTorch (Gardner et al., 2018). This model can also be interpreted as a Gaussian Process Latent Variable Model (GP-LVM). The GPyTorch implementation employs variational inference to learn hierarchical representations, making it particularly well-suited for high-dimensional and large-scale datasets. We omit the Deep Mahalanobis Gaussian Process (DMGP), as its performance is comparable to that of the doubly-stochastic DGP (de Souza et al., 2022), which is more commonly used as a benchmark in practice.

**Implementation, Initialization, and Hyperparameter Tuning** For each dataset setting, we repeat the experiment 10 times to account for randomness and report the averaged results. Hyperparameters are tuned using five-fold cross-validation on the training set, but only for the first run of each setting; the selected hyperparameters are then reused in the remaining runs to save experimentation time.

Specifically, the selected latent subspace dimension  $Q$  is selected from  $\{3, 5, 7\}$ , and the numbers of inducing points  $(L_1, L_2)$  for the function and projection matrices are chosen from a small predefined grid,  $\{2, 4, 6\} \times \{20, 40, 60\}$ . After cross-validation, each model is retrained on the full training set and evaluated on a held-out test set. To keep the cross-validation search space computationally feasible, we fix other tuning parameters such as the neighborhood size  $n$  and the number of Monte Carlo samples  $M_c$  to reasonable default values, and later perform sensitivity analyses to assess their influence on model performance. The local neighborhood size  $n$  is set according to the input dimension: we use  $n = 25$  for datasets with fewer than 30 input dimensions, and  $n = 35$  for higher-dimensional settings. While the original JGP paper (Park, 2022) recommends  $n \approx 15$ , we found that slightly larger neighborhoods improve numerical stability and predictive power in high-dimensional spaces, as also reflected in our experimental results. The number of Monte Carlo samples for prediction is set to  $M_c = 5$ , which we found sufficient for stable performance while keeping prediction time manageable. Since each Monte Carlo draw requires running a local JGP model for all test points, larger  $M_c$  values substantially increase inference time when the test set is large, so this choice represents a practical trade-off between accuracy and efficiency.

For variational optimization, we fix the learning rate  $\eta$  as 0.01 and run for 300 iterations. All parameters are initialized randomly, except for the covariance matrix  $(\Sigma_r^{(j)})$  of  $\mathbf{r}^{(j)}$ , which is initialized as  $U^T U$  with  $U$  as a randomly generated upper triangular matrix, to ensure positive definiteness and avoid numerical issues.

#### 4.1 Synthetic Datasets Construction

This section presents a series of simulated examples to demonstrate the effectiveness of the proposed DJGP model in comparison with the aforementioned baseline methods. The synthetic datasets are generated using a two-stage framework. In the first stage, we construct the latent feature space  $\mathcal{Z}$  of a dimension  $K$  and define the relationship between the response and the latent features, i.e., we generate  $\mathbf{y} = f(\mathbf{z}) + \epsilon$ . In the second stage, we apply different dimensionality expansion techniques by simulating the inverse of a smooth projection function  $g^{-1} : \mathcal{X} \rightarrow \mathcal{Z}$ , to lift the latent dimension  $K$  to dimension  $D$ . Therefore, the final dataset would have  $D$ -dimensional inputs.

As described in Section 4.1.1, in the first stage, we generate four synthetic datasets: L2 dataset with  $K = 2$ , which facilitates visualization of the relationship between the latent space and the response, and LH dataset with higher feature dimensions  $K = 4, 5, 7$ . For the second stage, we consider four different dimensionality expansion techniques, as described in Section 4.1.2. Depending on the choices in the two stages, we would have 16 different synthetic datasets.

##### 4.1.1 TOY EXAMPLES FOR LATENT SPACE MODELING

The toy examples used in the first stage are constructed as described below, with visualizations provided in Figure 1 to aid understanding.

- **L2 Dataset: Synthetic Phantom Dataset with 2-Dimensional Latent Space.** To illustrate DJGP’s ability to detect and model jumps, we begin with a two-dimensional toy example on the rectangle  $[-0.5, 0.5]^2$ , partitioned into two or more regions. Within each region  $k$ , the response surface is drawn from an independent GP with mean  $\mu_k$  (either 0 or 27) and squared-exponential covariance

$$c(\mathbf{z}, \mathbf{z}'; \theta_k) = \theta_{k1} \exp\left\{-\frac{1}{\theta_{k2}}(\mathbf{z} - \mathbf{z}')^\top (\mathbf{z} - \mathbf{z}')\right\},$$

where  $\theta_{k1} = 9$ ,  $\theta_{k2} = 200$ , and  $\mu_k \sim \text{Uniform}\{0, 27\}$ . Here, the length scale parameter  $\theta_{k2}$  is very large, which practically implies that the response surface is almost constant. This dataset basically emulates piecewise (nearly) constant response surfaces with random noises. A total of 1,100 data points are generated uniformly over the domain with additive Gaussian noise ( $\sigma^2 = 4$ ). From this pool, 100 points are randomly assigned to the test set, and the remaining 1000 are used for training.

- **LH Dataset: Synthetic Dataset with Higher-Dimensional Latent Space.** To evaluate scalability to higher intrinsic dimension, we generate data on  $[-0.5, 0.5]^K$  for  $K > 2$ . We define  $K + 1$  partitioning functions:

$$f_0(\mathbf{z}) = \sum_{i=1}^K z_i^2 - 0.4^2, \quad f_j(\mathbf{z}) = \sum_{i=1}^K z_i^2 - z_j^2 + (z_j + r_j \cdot 0.5)^2 - 0.3^2, \quad j = 1, \dots, K,$$

where each  $r_j$  is drawn uniformly from  $\{\pm 1\}$ . Each  $f_j$  bisects the domain into  $\mathcal{Z}_{j,+} = \{\mathbf{z} : f_j(\mathbf{z}) \geq 0\}$  and  $\mathcal{Z}_{j,-} = \{\mathbf{z} : f_j(\mathbf{z}) < 0\}$ . The region index is then

$$\text{region}(\mathbf{z}) = \sum_{j=0}^K 2^j \mathbb{I}_{\mathcal{Z}_{j,+}}(\mathbf{z}).$$

We draw  $N$  training points uniformly and sample responses from region-dependent GPs with mean  $\mu_k \sim \text{Uniform}\{-13.5k, +13.5k\}$  and squared-exponential covariance

$$c(\mathbf{z}, \mathbf{z}'; \theta_k) = \theta_{k1} \exp\left\{-\frac{1}{\theta_{k2}}(\mathbf{z} - \mathbf{z}')^\top(\mathbf{z} - \mathbf{z}')\right\},$$

using  $\theta_{k1} = 9$ ,  $\theta_{k2} = 200$ . We add zero-mean noise following  $\mathcal{N}(0, 4)$ . 100 test inputs are generated similarly without noise and constrained to lie within 0.05 of region boundaries.

#### 4.1.2 DIMENSION EXPANSION TECHNIQUES

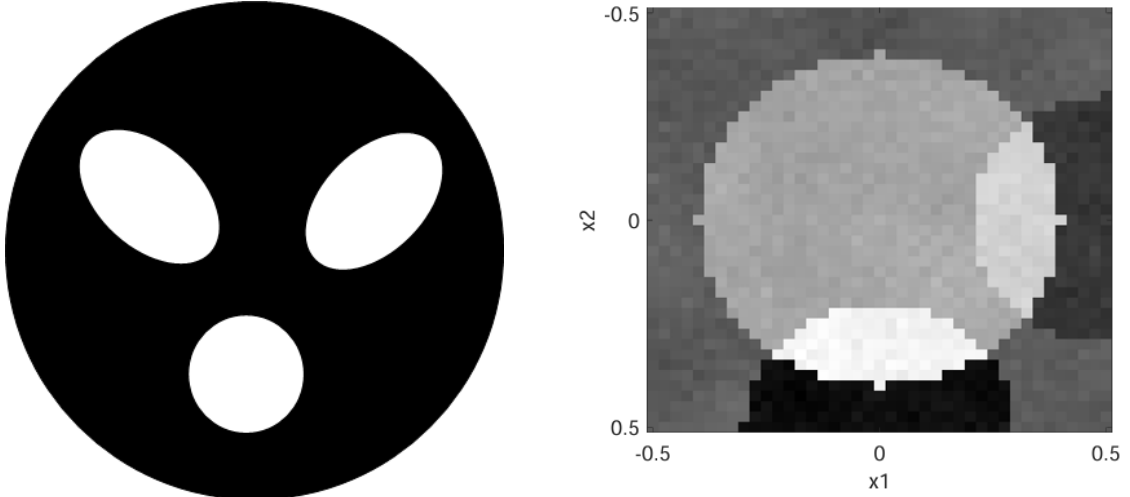
To investigate how different latent-to-observed mappings  $g$  affect the performance of various surrogate models, we design four distinct strategies for modeling the transformation from latent space to the observed input space:

- **Random Projection (RP):** To lift the latent representation of dimension  $K$  to a higher-dimensional space  $D$ , we generate a full-rank random projection matrix  $\mathbf{W} \in \mathbb{R}^{D \times K}$  with entries independently drawn from a standard Gaussian distribution. The resulting transformation is given by

$$\mathbf{x} = g^{-1}(\mathbf{z}) = \mathbf{W}\mathbf{z} \in \mathbb{R}^D.$$

- **Random Fourier Features (RF)**(Rahimi and Recht, 2007; Li et al., 2021): RF offers an efficient way to approximate shift-invariant kernels by mapping inputs into a randomized feature space. For RBF kernels, the mapping  $g : \mathbb{R}^K \rightarrow \mathbb{R}^{2D}$  is defined as:

$$g^{-1}(\mathbf{z}) := \frac{1}{\sqrt{D}} [\cos \langle \omega_1, \mathbf{z} \rangle, \sin \langle \omega_1, \mathbf{z} \rangle, \dots, \cos \langle \omega_D, \mathbf{z} \rangle, \sin \langle \omega_D, \mathbf{z} \rangle]^T,$$



(a) Ground-truth regression surface for L2 Dataset.

(b) Example realization from the LH dataset on the latent domain  $[-0.5, 0.5]^2$ , illustrating a high-dimensional projection to 2D latent space.

Figure 1: Illustrations of response surfaces over 2D latent spaces. (a) A noiseless ground-truth surface with sharp transitions from the L2 Dataset. (b) A simulated surface from the high-dimensional LH dataset projected onto 2D.

where  $\omega_i \sim \mathcal{N}(0, \sigma^{-2}I)$ . This yields an unbiased approximation to the RBF kernel:

$$k(\mathbf{z}_i, \mathbf{z}_j) = \exp\left(-\frac{\|\mathbf{z}_i - \mathbf{z}_j\|^2}{2\sigma^2}\right).$$

More generally, RF approximates any positive definite shift-invariant kernel using its Fourier transform. In our experiments, we use the following simplified form:

$$g^{-1}(\mathbf{z}) = \sqrt{\frac{2}{D}} \cos(\Omega\mathbf{z} + b),$$

where  $\Omega \in \mathbb{R}^{D \times K}$  is sampled from  $\mathcal{N}(0, I_K)$ , and  $b \in \mathbb{R}^D$  is drawn uniformly from  $[0, 2\pi]$ .

- **Polynomial Expansion (PE):** We enrich the latent representation by including all monomials of the original features up to degree three. This introduces smooth nonlinear interactions while maintaining a controlled feature dimensionality through truncation. Specifically, we define the expanded feature vector as

$$\mathbf{x} = \text{trunc}\left([z_1, \dots, z_K, z_1^2, z_1z_2, \dots, z_K^2, z_1^3, z_1^2z_2, \dots, z_K^3]\right),$$

where  $\mathbf{z} \in \mathbb{R}^K$  is the original latent vector, and *trunc* denotes selecting the first  $D$  components of the full polynomial basis in a fixed order (e.g., lexicographic).

- **Autoencoder (AE)**(Wang et al., 2016; Bank et al., 2023): We employ an overcomplete autoencoder to construct synthetic high-dimensional data from the low-dimensional latent variables  $\mathbf{z}$ . Unlike the typical use of autoencoders for dimensionality reduction, our architecture performs *dimension expansion*, mapping from  $K$  to  $D$  dimensions with  $D > K$ . Specifically, the encoder  $f_{\text{enc}} : \mathbb{R}^K \rightarrow \mathbb{R}^D$  defines the transformation from latent to observed space, and the decoder  $f_{\text{dec}} : \mathbb{R}^D \rightarrow \mathbb{R}^K$  reconstructs back to the latent domain.

The autoencoder is trained directly by minimizing the reconstruction loss  $\|\mathbf{z}_i - f_{\text{dec}}(f_{\text{enc}}(\mathbf{z}_i))\|_2^2$ , where  $\{\mathbf{z}_i\}_{i=1}^N$  represents the latent variable values generated by the simulation described in Section 4.1.1. After training, only the encoder is retained to generate the observed inputs  $\mathbf{x}_i = f_{\text{enc}}(\mathbf{z}_i)$  that serve as the training data for DJGP. Hence, DJGP receives only  $\mathbf{x}_i$  (without access to  $\mathbf{z}_i$ ) as input, making this setup a controlled dimension-expansion testbed for evaluating its ability to recover low-dimensional latent structure from high-dimensional data. Note that, unlike a conventional autoencoder used for dimensionality reduction, our *encoder* network acts as a generator that expands the low-dimensional latent variables  $\mathbf{z} \in \mathbb{R}^K$  into high-dimensional observations  $\mathbf{x} \in \mathbb{R}^D$  ( $D > K$ ), while the *decoder* reconstructs back to the latent domain. The encoder consists of a linear layer with 64 units, followed by BatchNorm and LeakyReLU, and a final linear layer projecting to  $D$ . The decoder mirrors this structure in reverse ( $D \rightarrow 64 \rightarrow K$ ) and omits the final activation. Batch normalization helps mitigate feature sparsity, while LeakyReLU prevents neuron “death.” The model is trained for 100 epochs.

## 4.2 Comparison to the Baseline Methods

Table 1 summarizes the average RMSE and CRPS performance of different surrogate models across various experimental settings. We also report rank scores based on both RMSE and CRPS. Note that the rank scores are computed across all repeated experiments by aggregating results from all dataset settings, thus providing a comprehensive overall ranking.

Table 1: Performance comparison of models on RMSE and CRPS

Dataset	D	K	N	n	Feature	MEAN RMSE					MEAN CRPS				
						DGP	JGP	JGP-SIR	JGP-AE	DJGP(Proposed)	DGP	JGP	JGP-SIR	JGP-AE	DJGP(Proposed)
L2	20	2	1k	25	AE	2.24	2.33	2.32	2.23	<b>2.21</b>	1.36	1.34	1.30	1.29	<b>1.29</b>
	20	2	1k	25	PE	2.33	2.23	2.32	<b>2.22</b>	2.26	1.42	<b>1.25</b>	1.31	1.26	1.27
	20	2	1k	25	RP	2.15	2.15	3.02	2.18	<b>2.15</b>	1.31	1.24	1.68	1.23	<b>1.22</b>
	20	2	1k	25	RF	<b>2.22</b>	2.26	2.41	2.24	2.27	1.34	1.28	1.34	1.26	<b>1.26</b>
LH	20	4	1k	25	AE	303.60	361.73	302.84	277.33	<b>271.39</b>	286.91	192.15	138.87	119.98	<b>114.09</b>
	20	4	1k	25	PE	314.39	290.50	<b>259.27</b>	266.15	292.97	297.39	126.00	<b>108.34</b>	111.56	117.51
	20	4	1k	25	RP	309.32	297.37	367.88	289.94	<b>283.60</b>	292.50	135.86	204.55	131.77	<b>125.55</b>
	20	4	1k	25	RF	303.19	303.00	295.86	324.80	<b>268.08</b>	287.15	137.99	127.83	162.07	<b>121.25</b>
LH	30	5	1k	25	AE	712.52	785.77	618.54	646.41	<b>563.89</b>	700.56	439.09	286.21	313.75	<b>248.25</b>
	30	5	1k	25	PE	727.80	706.05	<b>591.99</b>	636.41	604.33	714.77	347.64	<b>266.34</b>	304.36	270.85
	30	5	1k	25	RP	719.40	<b>642.72</b>	697.93	643.78	652.36	708.60	321.52	369.49	319.57	<b>317.46</b>
	30	5	1k	25	RF	711.81	711.40	611.26	656.97	<b>581.82</b>	701.22	364.36	284.54	318.57	<b>262.66</b>
LH	50	7	2k	35	AE	3099.28	2379.01	2488.79	2410.18	<b>1896.49</b>	3082.19	1060.76	1078.09	1044.05	<b>805.15</b>
	50	7	2k	35	PE	3123.36	2911.09	2497.91	2397.27	<b>2307.03</b>	3106.67	1471.66	1098.77	1022.11	<b>1019.60</b>
	50	7	2k	35	RP	3116.37	2508.01	2503.44	<b>2413.85</b>	2493.00	3100.04	1132.13	1115.80	<b>1047.43</b>	1099.38
	50	7	2k	35	RF	3109.00	2729.22	2482.38	2412.44	<b>2379.80</b>	3092.08	1300.04	1099.84	1047.86	<b>1011.23</b>
<b>RankScore</b>						4.13	3.38	3.19	2.44	<b>1.88</b>	4.88	3.44	3.06	2.13	<b>1.50</b>

*Note.* This table reports the mean RMSE and mean CRPS of different models across multiple datasets. Smaller values indicate better predictive performance. Here,  $D$  denotes the input dimension,  $K$  is the latent dimensionality used in dataset generation,  $N$  is the total number of training samples, and  $n$  denotes the local neighborhood size employed in the JGP-based methods.

We observe from Table 1 that across all experimental configurations, DJGP consistently achieves the best rank scores in both RMSE and CRPS, highlighting its superior predictive performance and well-calibrated uncertainty estimates.

Notably, DJGP consistently outperforms the original JGP, its dimension-reduced variants (JGP-SIR and JGP-AE), and the Deep Gaussian Process (DGP) in terms of RMSE and CRPS. Although JGP-SIR improves JGP, this advantage does not always persist in benchmark scenarios involving random projection (RP). This is reasonable, as RP is a linear transformation, and the lengthscale learning in JGP may already adapt effectively to linear structures in the input space, leaving little room for additional gains from applying SIR before JGP. In many tested scenarios, JGP-AE performs better than both JGP and JGP-SIR, owing to the autoencoder’s ability to capture complex nonlinear mappings between the original and latent spaces, thereby preserving richer information. Overall, DJGP attains the best performance among all benchmark methods in most scenarios and performs comparably to the best performers in the remainder, demonstrating its consistent effectiveness across diverse settings.

DGPs do not work very well particularly in terms of CRPS. This implies that while DGPs can fit the data well, they tend to make overconfident predictions and suffer from poor uncertainty calibration. This behavior highlights a key distinction between global models like DGPs and local models such as JGP or DJGP: global models learn a single, unified mapping across the entire input space, which can lead to poor adaptability in regions with abrupt changes. In contrast, local models adapt to specific regions of the input space, making them more robust to sharp transitions or jumps in the data. Furthermore, DGPs typically require large datasets to effectively learn hierarchical representations; with only  $N = 1000$  training points, their performance may be constrained by a small data size and an increased risk of overconfidence.

In summary, DJGP offers a compelling balance between accuracy and uncertainty estimation, and its robustness across various datasets and feature transformations demonstrates its effectiveness for high-dimensional, piecewise continuous surrogate modeling.

### 4.3 Effect of Latent Dimension $K$ , Observed Dimension $D$ , and Dataset Size $N$

To gain a deeper understanding of DJGP’s behavior under varying data conditions, we evaluate its predictive performance across different configurations. Specifically, we vary the latent dimension  $K$ , the observed (expanded) dimension  $D$ , and the number of training samples  $N$ . All experiments are conducted using the LH dataset with the RF expansion, although similar trends are observed with other datasets. We fixed  $J = 100$  and  $n = 35$ .

Figure 2 presents RMSE results for varying observed dimensions  $D$ , with fixed latent dimension  $K = 5$  and different training sizes  $N \in \{1000, 3000, 5000\}$ . RMSE does not consistently increase with higher observed dimensionality, suggesting that DJGP is capable of performing effective dimension reduction without incurring substantial information loss, even in high-dimensional input spaces.

Figure 3 shows the changes in RMSE as  $N$  increases while  $K$  is fixed to 3 or 5, and  $D$  fixed to 30. As the training size increases, the local neighborhoods become denser, which improves the quality of the local Taylor approximations applied in JGP and leads to a better predictive performance.

We also examined the RMSE trend of DJGP with varying latent dimensionality  $K \in \{3, \dots, 8\}$  and training sizes  $N \in \{1000, 3000, 5000, 10000\}$ , while keeping the original input dimension fixed at  $D = 30$ . Figure 4 (left) presents the mean RMSE as a function of  $N, K$ , while the right panel shows that RMSE scales approximately with  $N^{-K}$ , instead of  $N^{-D}$ . In other words, the RMSE

of DJGP follows a trend consistent with the theoretical error bound of a stationary GP applied to stationary data with input dimension  $K$  (Park, 2022), suggesting that DJGP effectively estimates the latent dimensionality and model nonstationarity and discontinuity in the data effectively.

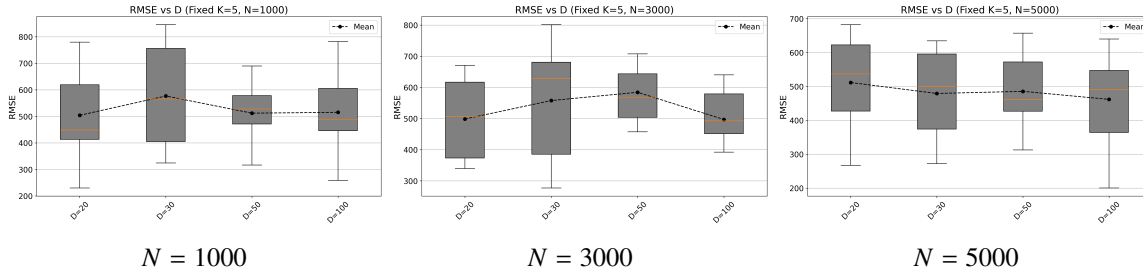


Figure 2: Effect of observed dimension  $D$  on RMSE under fixed latent dimension  $K = 5$  and varying training sizes. DJGP maintains stable performance even with increased dimensionality.

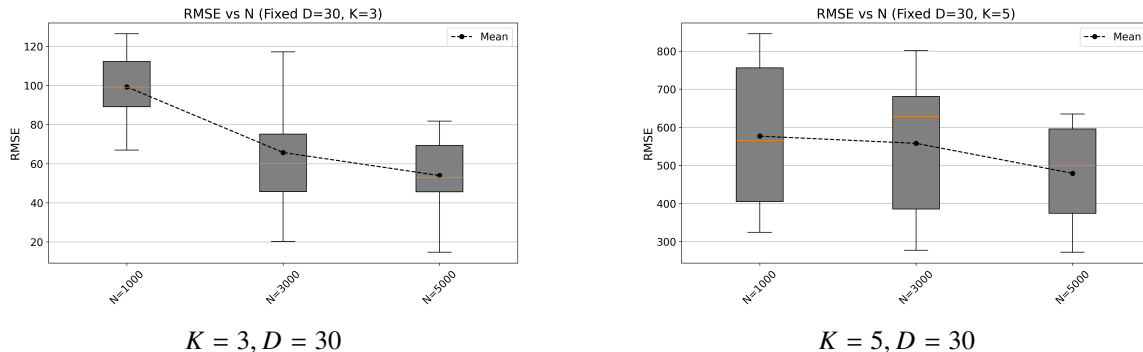


Figure 3: Effect of training set size  $N$  on RMSE under fixed observed dimension  $D = 30$  and different latent dimensions. Larger  $N$  leads to denser local neighborhoods and improved performance.

#### 4.4 Sensitivity to the Tuning Parameters

Selecting appropriate tuning parameters—such as the number of inducing points  $(L_1, L_2)$ , the neighborhood size  $n$ , and the latent dimension  $K$ —can be challenging, much like tuning a deep Gaussian process or deep neural network. In this section, we present a comprehensive hyperparameter sensitivity analysis using the LH dataset using RF expansion, with the goal of gaining deeper insights into DJGP’s behavior and providing practical guidance for selecting the tuning parameters.

##### 4.4.1 INFLUENCE OF NEIGHBORHOOD SIZE AND INDUCING POINTS

To examine the effect of the number of inducing points  $(L_1, L_2)$  on RMSE and CRPS, we conducted experiments on the LH dataset using fixed parameters  $(D, K, N, J) = (30, 5, 1000, 100)$ , while varying  $(L_1, L_2)$  over the grid  $\{2, 4, 6\} \times \{20, 40, 60\}$ .

Figure 5 displays heatmaps of (a) RMSE and (b) CRPS under different configurations. We observe that  $(L_1, L_2) = (4, 40)$  offers the best trade-off between accuracy and uncertainty calibration. When the number of local inducing points  $L_1$  is too small, the variational approximation becomes

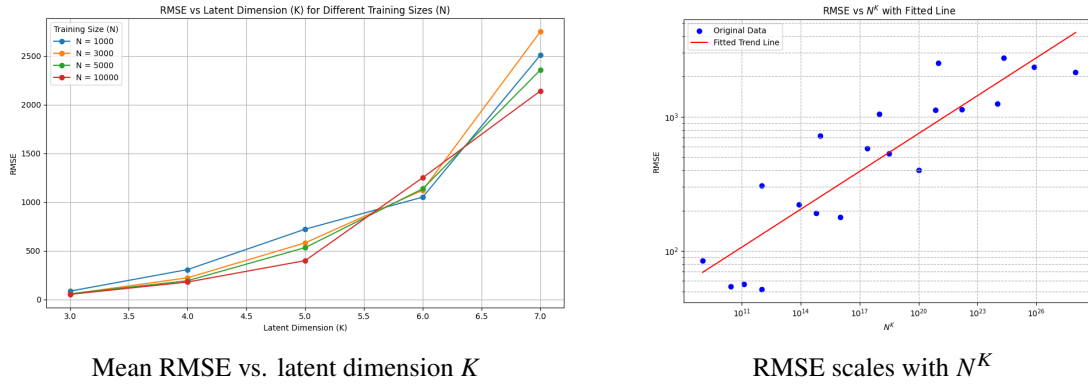


Figure 4: Effect of latent dimension  $K$  on DJGP performance. (Left) Mean RMSE as a function of the latent dimension  $K$  under varying sample sizes  $N$ . (Right) RMSE exhibits a scaling trend governed by  $N^K$  rather than  $N^D$ , consistent with the theoretical error behavior of stationary Gaussian processes with intrinsic input dimension  $K$  (Park, 2022). This indicates that DJGP effectively identifies the latent subspace and mitigates the curse of dimensionality in high-dimensional observations.

overly coarse. Increasing  $L_1$  generally improves performance by enhancing the expressiveness of the local variational distribution, but we observe diminishing returns beyond  $L_1 = 4$ , suggesting that a small number of inducing points is often sufficient. Increasing the number of global inducing points  $L_2$  generally improves performance, since a larger set of global points better approximates the nonlinear projection  $g(\cdot)$  with a number of locally linear projections. In practice, the optimal  $(L_1, L_2)$  depends on dataset-specific characteristics. We suggest to select them using cross-validation or a held-out validation set.

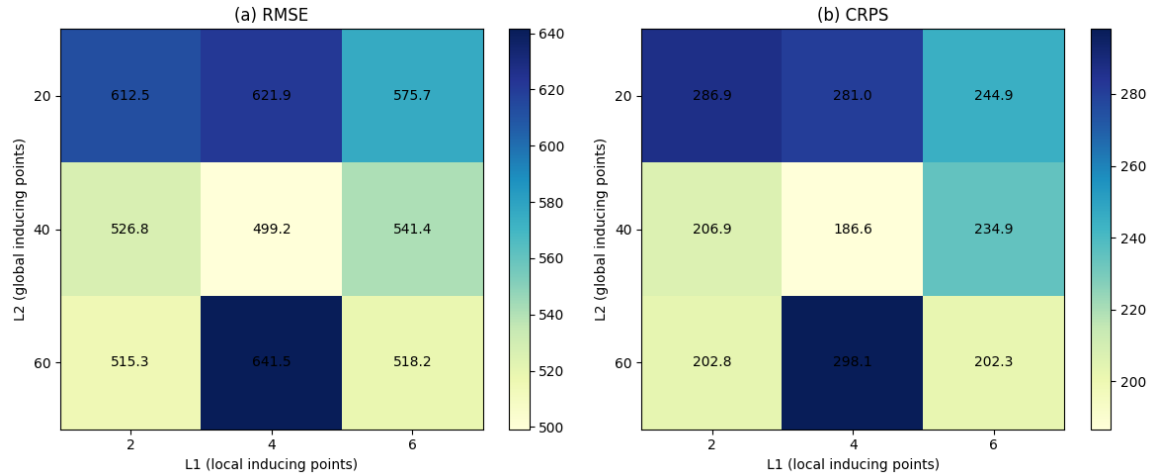


Figure 5: Effect of local and global inducing point counts  $(L_1, L_2)$  on (a) RMSE and (b) CRPS. The configuration  $(4, 40)$  achieves the best balance between predictive accuracy and uncertainty estimation.

Figure 6 further examines the joint influence of neighborhood size  $n$  and the number of local inducing points  $L_1$  on model performance. Both  $L_1$  and  $n$  are local hyperparameters that can interact: a larger  $n$  provides more local data, for which we may increase  $L_1$  to enable more expressive variational approximations of the local posterior distributions. However, an excessively large neighborhood size  $n$  would increase the approximation error of DJGP, as both the projection function and the JGP model rely on first-order Taylor approximations within each local neighborhood. When the local region becomes too wide, the approximation deviates more from the true function, enlarging the error bound and reducing predictive performance. According to Figure 6, when  $L_1 = 4$ , moderate neighborhood sizes—around  $n = 15$  and  $35$ —yield the lowest RMSE and CRPS.

Importantly, the optimal neighborhood size is dataset-dependent. For datasets with smooth latent structure and minimal discontinuities, larger neighborhoods can be beneficial. In contrast, for datasets with sharp discontinuities or frequent jump behavior, larger neighborhoods may introduce more heterogeneity, harming the quality of local approximations.

As a practical rule of thumb, for low-dimensional datasets ( $K \leq 10$ ), a neighborhood size in the range of 15–20 tends to perform well. For higher-dimensional datasets (e.g.,  $K > 10$ ), neighborhood sizes in the range of 25–35 are usually more appropriate to ensure sufficient data to estimate the increasing number of the local model parameters.

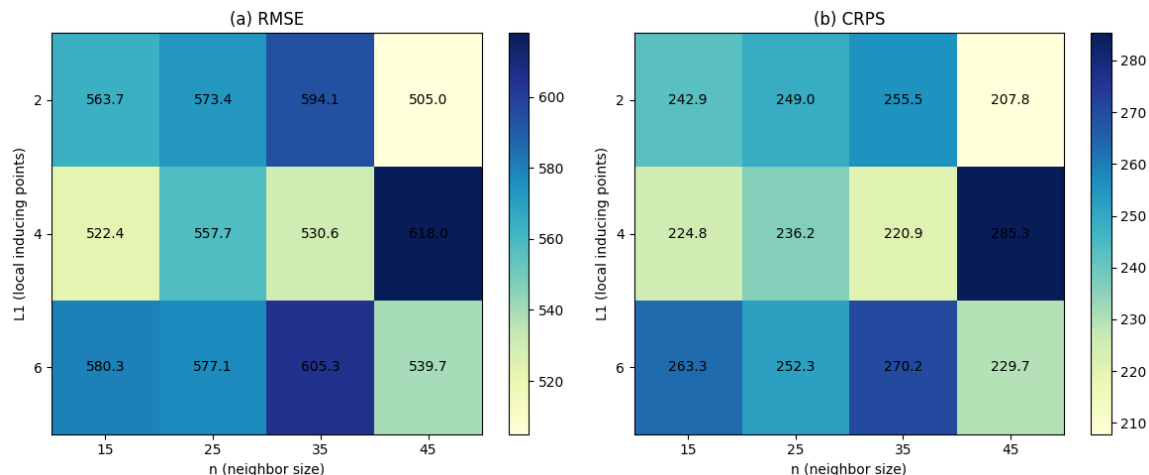


Figure 6: Joint effect of neighborhood size  $n$  (horizontal axis) and number of local inducing points  $L_1$  (vertical axis) on (a) RMSE and (b) CRPS.

#### 4.4.2 INFLUENCE OF SELECTED LATENT DIMENSION $Q$

We investigate how the choice of latent dimension  $Q$  influences the predictive performance of DJGP on the LH dataset using the RFF expansion method. This analysis aims to understand how the selected latent dimension, relative to the intrinsic dimensionality of the data, impacts model performance. To clearly distinguish between the two, we introduce a new symbol,  $Q$ , to denote the latent dimension actually used in the DJGP model, which may differ from the intrinsic latent dimension  $K$  employed in generating the synthetic dataset.

For this study, we still use the LH dataset. We fix  $N = 1000$ ,  $D = 30$ , and  $n = 35$ . We evaluate DJGP under various combinations of  $K \in \{2, 3, 5, 7\}$  and  $Q \in \{2, 3, 5, 7\}$ , and report the resulting RMSE and CRPS.

Figure 7 show the main results. We observe that an appropriate choice of  $Q$  can significantly improve RMSE. Specifically, moderate values of  $Q$  lead to lower prediction errors and reduced variability across different train–test splits. This trend is intuitive: when  $Q$  is too small, essential information may be lost in the projection, degrading model fidelity. Conversely, overly large  $Q$  increases latent space complexity, making region partitioning more difficult and leading to potential overfitting in the downstream Jump GP.

Interestingly, good performance is often achieved with  $Q = 3$  or  $Q = 5$ , regardless of the ground-truth  $K$ . For example, when  $K = 3$ , the best performance is observed at  $Q = 5$ , while when  $K = 7$ , a smaller  $Q = 3$  may still yield the lowest RMSE. This indicates that the optimal choice of  $Q$  does not necessarily coincide with the ground-truth latent dimension  $K$ . The optimal choice could be complicatedly related to multiple factors such as the intrinsic data dimension  $K$  and data size  $N$ . This would suggest that  $Q$  can be better chosen through the cross-validation.

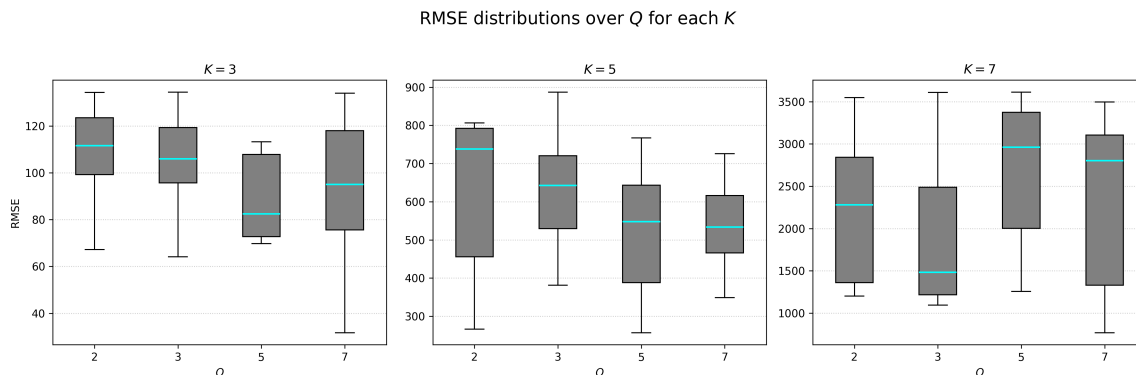


Figure 7: Effect of the target latent dimension  $Q$  on RMSE across different ground-truth latent dimensions  $K$ , evaluated on the LH dataset using RFF. Each box represents RMSE variation over 10 randomized train–test splits.

#### 4.4.3 GENERAL GUIDANCE ON HYPERPARAMETER SELECTION

Our model involves several hyperparameters, including the number of inducing points  $(L_1, L_2)$ , neighborhood size  $n$ , and target latent dimension  $Q$ , in addition to standard optimization parameters such as the learning rate and number of training epochs.

For model-specific hyperparameters, we adopt a unified strategy that combines empirical defaults with optional cross-validation for fine-tuning when computational resources permit. The neighborhood size  $n$ , the numbers of local and global inducing points  $(L_1, L_2)$ , and the target latent dimension  $Q$  jointly control the model’s locality, expressiveness, and projection capacity.

We find that setting  $n \in [25, 35]$ ,  $(L_1, L_2) = (4, 40)$ , and  $Q = 5$  provides a good balance between predictive accuracy and computational cost across our benchmark datasets. We suggest practitioners to use these values as default initializations, which can be further refined by cross-validation or validation-set tuning for new applications or when optimal performance is desired. In particular, we generally explore  $Q \in [3, 7]$ , as improvements tend to plateau beyond  $Q = 10$ . This approach

offers a consistent and reproducible starting point, while maintaining flexibility for dataset-specific adaptation.

Regarding optimization, we recommend fixing the learning rate at  $\eta = 0.01$  (or initializing at 0.1 with a cosine annealing schedule) based on validation performance on the LH dataset. A training duration of 200–300 epochs is typically sufficient, as further gains are usually realized in the subsequent JGP refinement stage. Training beyond 300 epochs rarely yields improvements and may lead to numerical instabilities, such as exploding gradients or ill-conditioned kernel matrices. For example, the model may exploit the ELBO objective via pathological solutions (so-called “ELBO hacking”) that artificially increase the variational bound without reducing RMSE, analogous to posterior collapse in VAEs (Lucas et al., 2019).

We also recommend using a held-out validation set to guide hyperparameter selection and to implement early stopping (e.g., halt if validation RMSE does not decrease for 20 consecutive epochs). This is important because the training objective (ELBO) does not always correlate with downstream metrics such as RMSE or CRPS. In our experience, ELBO may continue to improve even as validation RMSE increases, indicating overfitting to the variational bound. Note that validation incurs extra computational cost, so practitioners should balance this overhead against the benefits in their specific application.

In summary, the above configurations provide practical guidance for hyperparameter selection in the synthetic experiments and serve as effective initialization strategies for subsequent applications to real-world datasets.

## 5. Real Dataset Experiments

We evaluate DJGP and baseline models on three UCI regression benchmarks: Wine Quality, Parkinson’s Telemonitoring, and Appliances Energy Prediction. Table 2 summarizes key dataset statistics, including training set size  $N$ , input dimension  $D$ , test data size  $J$ , and the latent dimension applied in the model  $K$ . In addition, we compute three characteristics of each dataset: average gradient magnitudes ( $G_a$ ), maximum gradient magnitudes ( $G_m$ ), and the second-order total variation  $TV_2$ . We follow (Heinonen, 2001) to define  $G_a$  and  $G_m$  as:  $G_a = \frac{1}{|\mathcal{E}|} \sum_{(i,j) \in \mathcal{E}} \frac{|y_i - y_j|}{\|x_i - x_j\|}$ ,  $G_m = \max_{(i,j) \in \mathcal{E}} \frac{|y_i - y_j|}{\|x_i - x_j\|}$ : average and maximum local gradient magnitudes, where  $\mathcal{E}$  is the set of all the edges of a  $k$ -nearest neighbor graph ( $k = 6$ ) of the training data, and the neighborhood is defined as the proximity in the input space.

The second-order total variation  $TV_2$  is defined as below: first project the original inputs  $x_i$  onto the first principal component and use the resulting principal component scores to sort the training data by the increasing order of the scores. Let  $y_{(1)}, y_{(2)}, \dots, y_{(N)}$  be the sorted response variable values. The total variation is defined as

$$TV_2 = \sum_{i=2}^{n-1} |(y_{(i+1)} - y_{(i)}) - (y_{(i)} - y_{(i-1)})|.$$

This projection-based definition provides a consistent one-dimensional proxy for measuring the overall roughness of the regression function in high-dimensional settings. These quantities provide insights into the noisiness and non-smoothness of the regression functions.

From Table 2, we observe that:

- **Wine Quality** has the lowest input dimension and the lowest average gradient magnitude, indicating relatively smooth behavior and low functional complexity.
- **Parkinson’s Telemonitoring** has moderate dimensionality but a much higher  $TV_2$ , suggesting more nonlinear transitions or irregularities, despite modest average gradients.
- **Appliances Energy Prediction** exhibits the highest dimensionality and largest training set. Both its average and maximum local gradients, as well as  $TV_2$ , are substantially larger, pointing to high complexity and strong nonstationarity.

Furthermore, all three datasets exhibit significantly higher maximum gradients than their respective averages, suggesting the presence of local discontinuities or sharp transitions—highlighting the need for flexible models that can accommodate heterogeneous behaviors.

We target a held-out test-set size of roughly 10% of the data for the smaller datasets (the Wine Quality and Parkinson’s datasets). For the larger Appliances dataset ( $\approx 20,000$  samples), we fix the test set size at approximately 600 points to ensure comparable evaluation costs across methods. Since DJGP and its baseline models rely on local or Monte Carlo-based inference at each test input, the total prediction time scales roughly linearly with the number of test points. Fixing the test set size thus maintains similar computational budgets for all models. All dataset splits are repeated over 10 random seeds, and the reported results are averaged across these runs. Unless otherwise specified, the latent dimension  $K$  for each method is selected using five-fold cross-validation on one random split, and the same choice is applied for the other nine random splits. For DGP,  $K$  refers to the dimensionality of the latent space in the final hidden layer. All models are trained with a fixed learning rate of 0.01, and early stopping is applied based on performance on a 10% validation subset of the training data (i.e., training terminates when validation error no longer improves). For DJGP, we adopt the recommended settings from Section 4.4:  $(L_1, L_2) = (4, 40)$ , neighborhood size  $n = 35$ , and Monte Carlo sample sizes  $M_c = 3$ .

Table 2: Dataset statistics and smoothness metrics.

Dataset	$N$	$D$	$J$	$K$	$G_a$	$G_m$	$TV_2$
Wine Quality	6,497	11	650	3	0.327	9.90	8,798
Parkinson’s Telemonitoring	5,875	19	588	5	2.685	56.83	60,872
Appliances Energy Prediction	19,735	28	593	5	6.459	355.17	2,849,220

Figures 8 show the distribution of RMSE and CRPS across 10 randomized train–test splits. Overall, JGP-based models consistently outperform DGP, supporting the hypothesis that local models are better suited for handling heterogeneous structures and potential discontinuities. DJGP consistently achieves the best performance across all datasets, excelling in both RMSE and CRPS. On the **Wine Quality** dataset, DJGP achieves the lowest median RMSE while the RMSE metric has relatively higher variations—attributable to the stochasticity introduced by sampling latent projection matrices during inference. On the **Parkinson’s Telemonitoring** dataset, where PCA, SIR, and AE all degrade the performance of vanilla JGP, DJGP significantly outperforms all baselines. This highlights the advantage of its integrated dimensionality reduction, which avoids the information loss often introduced by two-stage projection methods. On the most challenging dataset—**Appliances Energy Prediction**—which is both high-dimensional and structurally irregular, DJGP delivers substantial

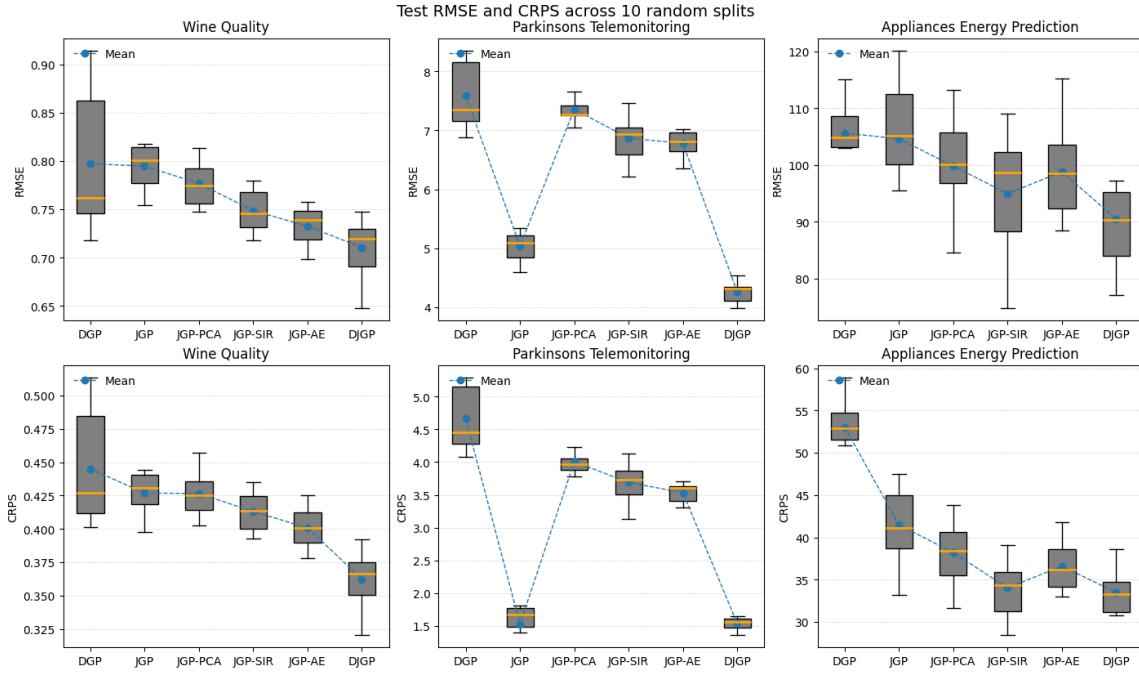


Figure 8: Predictive performance comparison across real datasets.

performance gains, demonstrating its scalability and robustness in large-scale, complex regression settings.

DGP, although theoretically capable of modeling nonstationarity, exhibits the weakest performance overall. Its underperformance is likely due to a mismatch between its smooth functional assumptions and the presence of jump discontinuities or outliers. DGP also shows higher variability on the smaller Wine and Parkinson’s datasets, suggesting it is more data-hungry and less robust in low-data regimes.

Table 3 reports average runtime. JGP-SIR and JGP-PCA benefit from dimensionality reduction, running much faster than JGP. DJGP incurs moderate overhead due to Monte Carlo sampling of projections and repeated local GP inference. Nonetheless, its runtime remains comparable to or lower than DGP, particularly on the large Appliances dataset. DGP exhibits the highest computational cost, stemming from its global variational updates over the entire dataset.

Dataset	DGP	JGP	JGP-SIR	JGP-PCA	JGP-AE	DJGP <sub>tr</sub>	DJGP <sub>inf</sub>	DJGP <sub>tot</sub>
Wine Quality	179.2	173.1	31.3	32.5	160.9	104.9	97.5	202.4
Parkinson’s Telemonitoring	279.4	384.3	49.7	49.9	206.5	244.0	149.7	393.7
Appliances Energy Prediction	968.2	632.9	52.7	55.7	268.0	199.3	167.1	366.4

Table 3: Average runtime (in seconds) for each method. DJGP<sub>tr</sub>, DJGP<sub>inf</sub>, and DJGP<sub>tot</sub> denote training time, inference time, and total runtime, respectively.

## 6. Conclusion

We have introduced the Deep Jump Gaussian Process (DJGP), a novel surrogate model that unifies global subspace learning with local discontinuity detection. By placing Gaussian-process priors on region-specific projection matrices and incorporating this region-specific dimension reduction schemes into JGP, DJGP jointly discovers low-dimensional feature mappings and piecewise-continuous regimes in high-dimensional inputs. Our gradient-based variational inference algorithm simultaneously optimizes the region-specific projection parameters, local JGP hyperparameters, and partitioning schemes, leveraging inducing-point approximations to maintain computational tractability.

Through extensive experiments on simulated benchmarks and three real-world UCI datasets, we have shown that DJGP consistently attains lower RMSE and CRPS than competing methods, including JGP with no dimension reduction, JGP with PCA or SIR as a dimension reduction method, and two-layer deep GPs. The integrated dimensionality reduction in DJGP prevents overfitting in local neighborhoods and yields more reliable partition boundaries in sparse, high-dimensional spaces.

DJGP’s ability to capture abrupt regime changes with the capability of uncertainty quantification makes it well suited for applications ranging from material science (where phase transitions occur) to econometrics and social-science studies (where treatment effects shift across subpopulations). Future work will explore online extensions for streaming data, richer partitioning functions within learned subspaces, and modeling of multi-modal discontinuities in complex engineering systems.

## References

- Hervé Abdi and Lynne J Williams. Principal component analysis. *Wiley Interdisciplinary Reviews: Computational Statistics*, 2(4):433–459, 2010.
- Titsias RC AUEB, Miguel Lázaro-Gredilla, et al. Variational inference for Mahalanobis distance metrics in Gaussian process regression. *Advances in Neural Information Processing Systems*, 26, 2013.
- Mukund Balasubramanian and Eric L Schwartz. The isomap algorithm and topological stability. *Science*, 295(5552):7–7, 2002.
- Dor Bank, Noam Koenigstein, and Raja Giryes. Autoencoders. *Machine Learning for Data Science Handbook: Data Mining and Knowledge Discovery Handbook*, pages 353–374, 2023.
- Jean-Paul Chiles and Pierre Delfiner. *Geostatistics: modeling spatial uncertainty*. John Wiley & Sons, 2012.
- Zhenwen Dai, Andreas Damianou, Javier González, and Neil Lawrence. Variational auto-encoded deep Gaussian processes. *arXiv preprint arXiv:1511.06455*, 2015.
- Andreas Damianou. *Deep Gaussian processes and variational propagation of uncertainty*. PhD thesis, University of Sheffield, 2015.
- Andreas Damianou and Neil D Lawrence. Deep Gaussian processes. In *Artificial Intelligence and Statistics*, pages 207–215. PMLR, 2013.
- Andreas Damianou, Michalis Titsias, and Neil Lawrence. Variational Gaussian process dynamical systems. *Advances in Neural Information Processing Systems*, 24, 2011.

- Daniel Augusto de Souza, Diego Mesquita, César Lincoln Mattos, and João Paulo Gomes. Deep Mahalanobis Gaussian process. In *Proceedings of the NeurIPS Workshop on Gaussian Processes, Spatiotemporal Modeling, and Decision-making Systems*, 2022.
- Jacob Gardner, Geoff Pleiss, Kilian Q Weinberger, David Bindel, and Andrew G Wilson. Gpytorch: Blackbox matrix-matrix Gaussian process inference with gpu acceleration. *Advances in Neural Information Processing Systems*, 31, 2018.
- RB Gramacy, J Niemi, and RM Weiss. Massively parallel approximate Gaussian process regression. *SIAM/ASA Journal on Uncertainty Quantification*, 2(1):564–584, 2014.
- Robert B Gramacy. *Surrogates: Gaussian process modeling, design, and optimization for the applied sciences*. Chapman and Hall/CRC, 2020.
- Robert B Gramacy and Daniel W Apley. Local Gaussian process approximation for large computer experiments. *Journal of Computational and Graphical Statistics*, 24(2):561–578, 2015.
- Robert B Gramacy and Herbert K H Lee. Bayesian treed Gaussian process models with an application to computer modeling. *Journal of the American Statistical Association*, 103(483):1119–1130, 2008.
- Marton Havasi, José Miguel Hernández-Lobato, and Juan José Murillo-Fuentes. Inference in deep Gaussian processes using stochastic gradient hamiltonian monte carlo. *Advances in Neural Information Processing Systems*, 31, 2018.
- Juha Heinonen. *Lectures on analysis on metric spaces*. Springer Science & Business Media, 2001.
- Markus Heinonen, Henrik Mannerström, Juho Rousu, Samuel Kaski, and Harri Lähdesmäki. Non-stationary Gaussian process regression with hamiltonian monte carlo. In *Artificial Intelligence and Statistics*, pages 732–740. PMLR, 2016.
- James Hensman, Nicolo Fusi, and Neil D Lawrence. Gaussian processes for big data. *arXiv preprint arXiv:1309.6835*, 2013.
- Yicheng Kang, Xiaodong Gong, Jiti Gao, and Peihua Qiu. Errors-in-variables jump regression using local clustering. *Statistics in Medicine*, 38(19):3642–3655, 2019.
- Kristian Kersting, Christian Plagemann, Patrick Pfaff, and Wolfram Burgard. Most likely heteroscedastic Gaussian process regression. In *Proceedings of the 24th International Conference on Machine Learning*, pages 393–400, 2007.
- Hyoung-Moon Kim, Bani K Mallick, and Chris C Holmes. Analyzing nonstationary spatial data using piecewise Gaussian processes. *Journal of the American Statistical Association*, 100(470):653–668, 2005.
- Diederik P. Kingma, Shakir Mohamed, Danilo J. Rezende, and Max Welling. Semi-supervised learning with deep generative models. In *Advances in Neural Information Processing Systems*, pages 3581—3589, 2014.

- Bledar A Konomi, Huiyan Sang, and Bani K Mallick. Adaptive bayesian nonstationary modeling for large spatial datasets using covariance approximations. *Journal of Computational and Graphical Statistics*, 23(3):802–829, 2014.
- Neil D Lawrence and Andrew J Moore. Hierarchical Gaussian process latent variable models. In *Proceedings of the 24th International Conference on Machine Learning*, pages 481–488, 2007.
- Lei Le, Andrew Patterson, and Martha White. Supervised autoencoders: Improving generalization performance with unsupervised regularizers. In *Advances in Neural Information Processing Systems*, volume 31, pages 107—117, 2018.
- Jaehoon Lee, Yasaman Bahri, Roman Novak, Samuel S Schoenholz, Jeffrey Pennington, and Jascha Sohl-Dickstein. Deep neural networks as Gaussian processes. *arXiv preprint arXiv:1711.00165*, 2017.
- Ker-Chau Li. Sliced inverse regression for dimension reduction. *Journal of the American Statistical Association*, 86(414):316–327, 1991.
- Zhu Li, Jean-Francois Ton, Dino Oglic, and Dino Sejdinovic. Towards a unified analysis of random fourier features. *Journal of Machine Learning Research*, 22(108):1–51, 2021.
- James Lucas, George Tucker, Roger B Grosse, and Mohammad Norouzi. Don’t blame the elbo! a linear vae perspective on posterior collapse. *Advances in Neural Information Processing Systems*, 32, 2019.
- Zhao Tang Luo, Huiyan Sang, and Bani Mallick. A bayesian contiguous partitioning method for learning clustered latent variables. *Journal of Machine Learning Research*, 22(37):1–52, 2021.
- Laurens van der Maaten and Geoffrey Hinton. Visualizing data using t-sne. *Journal of machine learning research*, 9(Nov):2579–2605, 2008.
- Alireza Makhzani and Brendan J. Frey. Winner-take-all autoencoders. In *Advances in Neural Information Processing Systems*, volume 28, pages 2791—2799, 2015.
- Christopher Paciorek and Mark Schervish. Nonstationary covariance functions for Gaussian process regression. *Advances in Neural Information Processing Systems*, 16, 2003.
- Chiwoo Park. Jump Gaussian process model for estimating piecewise continuous regression functions. *Journal of Machine Learning Research*, 23(278):1–37, 2022.
- Chiwoo Park, Peihua Qiu, Jennifer Carpena-Núñez, Rahul Rao, Michael Susner, and Benji Maruyama. Sequential adaptive design for jump regression estimation. *IJSE Transactions*, 55(2):111–128, 2022.
- Christopher A Pope, John Paul Gosling, Stuart Barber, Jill S Johnson, Takanobu Yamaguchi, Graham Feingold, and Paul G Blackwell. Gaussian process modeling of heterogeneity and discontinuities using voronoi tessellations. *Technometrics*, 63(1):53–63, 2021.
- Peihua Qiu. Jump-preserving surface reconstruction from noisy data. *Annals of the Institute of Statistical Mathematics*, 61:715–751, 2009.

- Novi Quadrianto, Kristian Kersting, Mark D Reid, Tibério S Caetano, and Wray L Buntine. Kernel conditional quantile estimation via reduction revisited. In *2009 Ninth IEEE International Conference on Data Mining*, pages 938–943. IEEE, 2009.
- Ali Rahimi and Benjamin Recht. Random features for large-scale kernel machines. *Advances in Neural Information Processing Systems*, 20, 2007.
- Paul D Sampson and Peter Guttorp. Nonparametric estimation of nonstationary spatial covariance structure. *Journal of the American Statistical Association*, 87(417):108–119, 1992.
- Thomas J Santner, Brian J Williams, William I Notz, and Brian J Williams. *The design and analysis of computer experiments*, volume 1. Springer, 2003.
- Annie Sauer, Andrew Cooper, and Robert B. Gramacy. Vecchia-approximated deep Gaussian processes for computer experiments. *Journal of Computational and Graphical Statistics*, 32(3): 824–837, 2023a. doi: 10.1080/10618600.2022.2129662.
- Annie Sauer, Andrew Cooper, and Robert B Gramacy. Non-stationary Gaussian process surrogates. *arXiv preprint arXiv:2305.19242*, 2023b.
- Lawrence K Saul and Sam T Roweis. An introduction to locally linear embedding. *unpublished*. Available at: <http://www.cs.toronto.edu/~roweis/lle/publications.html>, 2000.
- Bernhard Schölkopf, Alexander Smola, and Klaus-Robert Müller. Kernel principal component analysis. In *International conference on artificial neural networks*, pages 583–588. Springer, 1997.
- Kihyuk Sohn, Honglak Lee, and Xinchun Yan. Learning structured output representation using deep conditional generative models. In *Advances in Neural Information Processing Systems*, pages 3483—3491, 2015.
- Matthew A Taddy, Robert B Gramacy, and Nicholas G Polson. Dynamic trees for learning and design. *Journal of the American Statistical Association*, 106(493):109–123, 2011.
- Michalis Titsias. Variational learning of inducing variables in sparse Gaussian processes. In *Artificial Intelligence and Statistics*, pages 567–574. PMLR, 2009.
- Michalis Titsias and Neil D Lawrence. Bayesian Gaussian process latent variable model. In *Proceedings of the Thirteenth International Conference on Artificial Intelligence and Statistics*, pages 844–851. JMLR Workshop and Conference Proceedings, 2010.
- Ville Tolvanen, Pasi Jylänki, and Aki Vehtari. Expectation propagation for nonstationary heteroscedastic Gaussian process regression. In *2014 IEEE International Workshop on Machine Learning for Signal Processing (MLSP)*, pages 1–6. IEEE, 2014.
- Yasi Wang, Hongxun Yao, and Sicheng Zhao. Auto-encoder based dimensionality reduction. *Neurocomputing*, 184:232–242, 2016.
- Holger Wendland. *Scattered data approximation*, volume 17. Cambridge University Press, 2004.
- Andrew G Wilson, Zhiting Hu, Russ R Salakhutdinov, and Eric P Xing. Stochastic variational deep kernel learning. *Advances in Neural Information Processing Systems*, 29, 2016a.

Andrew Gordon Wilson, Zhiting Hu, Ruslan Salakhutdinov, and Eric P Xing. Deep kernel learning. In *Artificial Intelligence and Statistics*, pages 370–378. PMLR, 2016b.

## Appendices

### A. Variational Inference

#### Notation

For clarity, we summarize the main symbols and notations used throughout the paper in Table 4. The table lists the definition and dimension of each quantity, including input variables, local and global projection matrices, inducing variables, kernel matrices, and hyperparameters. This serves as a reference for both the main text and the derivations in the appendix.

Table 4: Summary of notation used throughout the paper.

Symbol	Description	Dimension
$\mathbf{x}_i^{(j)}$	Input feature of sample $i$ in region $j$	$\mathbb{R}^D$
$\mathbf{y}^{(j)}$	Output vector in region $j$	$\mathbb{R}^n$
$K$	Latent dimension of projection space	scalar
$D$	Input dimension	scalar
$J$	Number of local regions	scalar
$n$	Local neighborhood size	scalar
$Q$	Target latent dimension of projection space in DJGP	scalar
$N$	Total number of training data points	scalar
$\mathbf{W}_j$	Local projection matrix at region $j$	$\mathbb{R}^{K \times D}$
$w_{kd}^{(j)}$	Entry $(k, d)$ of $\mathbf{W}_j$	scalar
$\mathbf{R}_\ell$	Global inducing output at inducing input $\tilde{\mathbf{x}}_\ell$	$\mathbb{R}^{K \times D}$
$R_{lkd}$	Entry $(k, d)$ of $\mathbf{R}_\ell$	scalar
$v_i^{(j)}$	Latent indicator for sample $i$ in region $j$	$\{0, 1\}$
$\mathbf{r}^{(j)}$	Inducing variables for region $j$	$\mathbb{R}^m$
$q(\mathbf{r}^{(j)})$	Variational posterior over $\mathbf{r}^{(j)}$	Gaussian
$q(v_i^{(j)})$	Variational posterior over $v_i^{(j)}$	Bernoulli
$q(R_{lkd})$	Variational posterior of $R_{lkd}$	$\mathcal{N}(\mu_{lkd}, \sigma_{lkd}^2)$
$\mathbf{K}_r^{(j)}$	Kernel matrix among local inducing points in region $j$	$\mathbb{R}^{L_1 \times L_1}$
$\mathbf{K}_{fr}^{(i,j)}$	Cross-covariance between $f_i$ and local inducing points	$\mathbb{R}^{1 \times L_1}$
$\mathbf{K}_{rf}^{(i,j)}$	Cross-covariance transpose	$\mathbb{R}^{L_1 \times 1}$
$\Psi_1$	Expectation $\langle \mathbf{K}_{fr} \rangle_{q(\mathbf{W})}$	$\mathbb{R}^{n \times L_1}$
$\Psi_2^{(i)}$	Expectation $\langle \mathbf{K}_{rf}^{(i)} \mathbf{K}_{fr}^{(i)} \rangle_{q(\mathbf{W})}$	$\mathbb{R}^{L_1 \times L_1}$
$\sigma_j^2$	Noise variance in region $j$	scalar
$\sigma_{lkd}^2$	Variance parameter of $q(R_{lkd})$	scalar
$\ell_{w,k}$	Lengthscale of GP prior for dimension $k$	scalar
$s^2$	Signal variance of $\mathbf{W}$	scalar

In this appendix, we provide the full derivation of the evidence lower bound (ELBO) for the DJGP model, using the notation and variational family adopted in the main text. Throughout,  $j \in \{1, \dots, J\}$  indexes test regions,  $i \in \mathcal{D}_n^{(j)}$  indexes local neighbors,  $\ell \in \{1, \dots, L_1\}$  (local inducing) and  $\ell \in \{1, \dots, L_2\}$  (global inducing),  $k \in \{1, \dots, K\}$  indexes latent coordinates, and  $d \in \{1, \dots, D\}$  indexes observed dimensions.

**Variational factorization.** We approximate the posterior by

$$q(\{\mathbf{f}^{(j)}, \mathbf{r}^{(j)}, \mathbf{v}^{(j)}, \mathbf{W}_j\}_{j=1}^J, \mathbf{R}) = \prod_{j=1}^J \left[ p(\mathbf{f}^{(j)} \mid \mathbf{r}^{(j)}, \mathbf{W}_j, \Theta^{(j)}) q(\mathbf{r}^{(j)}) \prod_{i \in \mathcal{D}_n^{(j)}} q(v_i^{(j)}) \right] p(\mathbf{W} \mid \mathbf{R}, \Theta_W) q(\mathbf{R}),$$

with

$$q(\mathbf{r}^{(j)}) = \mathcal{N}(\boldsymbol{\mu}_r^{(j)}, \boldsymbol{\Sigma}_r^{(j)}), \quad q(v_i^{(j)}) = \text{Bernoulli}(\rho_i^{(j)}),$$

and the **mean-field per-element** global inducing posterior

$$q(\mathbf{R}) = \prod_{\ell=1}^{L_2} \prod_{k=1}^K \prod_{d=1}^D \mathcal{N}(R_{\ell,k,d} \mid \mu_{\ell kd}, \sigma_{\ell kd}^2).$$

**Variational distribution of  $\mathbf{W}$ .** We do not introduce an explicit variational factor for the projection matrices  $\mathbf{W}$ . Instead,  $\mathbf{W}$  follows the conditional GP prior  $p(\mathbf{W} \mid \mathbf{R}, \Theta_W)$  under the global variational posterior  $q(\mathbf{R})$ :

$$q(\mathbf{W}) = \mathbb{E}_{q(\mathbf{R})} [p(\mathbf{W} \mid \mathbf{R}, \Theta_W)] = \prod_{j=1}^J \mathbb{E}_{q(\mathbf{R})} [p(\mathbf{W}_j \mid \mathbf{R}, \Theta_W)]. \quad (21)$$

Given  $\mathbf{R}$ , the local projections  $\{\mathbf{W}_j\}_{j=1}^J$  are conditionally independent. Because both  $p(\mathbf{W} \mid \mathbf{R}, \Theta_W)$  and  $q(\mathbf{R})$  are Gaussian, the induced marginal  $q(\mathbf{W})$  and each  $q(\mathbf{W}_j)$  are also Gaussian.

**Induced marginal  $q(\mathbf{W}_j)$  and its moments.** Under the global GP prior

$$p(\mathbf{W} \mid \Theta_W) = \prod_{k=1}^K \prod_{d=1}^D \mathcal{N}(\mathbf{w}_{kd} \mid \mathbf{0}_J, \mathbf{C}_w^{(k)}), \quad (22)$$

each coordinate process  $\mathbf{w}_{kd} = [w_{kd}^{(1)}, \dots, w_{kd}^{(J)}]^\top$  is a zero-mean Gaussian process with covariance  $[\mathbf{C}_w^{(k)}]_{jj'} = s^2 \exp(-\frac{1}{2} \|\mathbf{x}_*^{(j)} - \mathbf{x}_*^{(j')}\|^2 / \ell_{w,k}^2)$ , where  $\Theta_W = (s, \ell_{w,1}, \dots, \ell_{w,K})$ . Let  $\mathbf{R}_{:kd} = [R_{1kd}, \dots, R_{L_2 kd}]^\top$  denote the global inducing outputs at inducing inputs  $\{\tilde{\mathbf{x}}_\ell\}_{\ell=1}^{L_2}$  with covariance  $\mathbf{K}_{RR}^{(k)}$  and cross-covariance  $\mathbf{K}_{jR}^{(k)} = [C(\mathbf{x}_*^{(j)}, \tilde{\mathbf{x}}_1), \dots, C(\mathbf{x}_*^{(j)}, \tilde{\mathbf{x}}_{L_2})]$ . Then the conditional GP prior for each element  $w_{kd}^{(j)}$  given  $\mathbf{R}_{:kd}$  is

$$p(w_{kd}^{(j)} \mid \mathbf{R}_{:kd}, \Theta_W) = \mathcal{N}\left(\mathbf{K}_{jR}^{(k)} (\mathbf{K}_{RR}^{(k)})^{-1} \mathbf{R}_{:kd}, s^2 - \mathbf{K}_{jR}^{(k)} (\mathbf{K}_{RR}^{(k)})^{-1} \mathbf{K}_{jR}^{(k)}\right). \quad (23)$$

Integrating out  $\mathbf{R}$  under the Gaussian  $q(\mathbf{R})$  yields the marginal

$$q(\mathbf{W}_j) = \int p(\mathbf{W}_j \mid \mathbf{R}, \Theta_W) q(\mathbf{R}) d\mathbf{R} = \mathcal{N}(\mathbf{W}_j \mid \boldsymbol{\mu}_W^{(j)}, \boldsymbol{\Sigma}_W^{(j)}), \quad (24)$$

whose moments follow from the conditional–Gaussian propagation formulas:

$$\begin{aligned}\boldsymbol{\mu}_W^{(j)}(k, d) &= \mathbf{K}_{jR}^{(k)} (\mathbf{K}_{RR}^{(k)})^{-1} \boldsymbol{\mu}_{kd}, \\ \boldsymbol{\Sigma}_W^{(j)}(k, d) &= s^2 - \mathbf{K}_{jR}^{(k)} (\mathbf{K}_{RR}^{(k)})^{-1} \mathbf{K}_{Rj}^{(k)} + \mathbf{K}_{jR}^{(k)} (\mathbf{K}_{RR}^{(k)})^{-1} \boldsymbol{\Sigma}_{kd} (\mathbf{K}_{RR}^{(k)})^{-1} \mathbf{K}_{Rj}^{(k)},\end{aligned}\tag{25}$$

where  $\boldsymbol{\mu}_{kd}$  and  $\boldsymbol{\Sigma}_{kd}$  are the mean vector and diagonal covariance of  $q(\mathbf{R}_{:kd})$  as defined in the previous subsection.

**ELBO decomposition.** Using Jensen’s inequality, the evidence lower bound (ELBO) can be written as

$$\begin{aligned}\mathcal{L} &= \sum_{j=1}^J \underbrace{\left( \mathbb{E}_j \left[ \log p(\mathbf{y}^{(j)} \mid \mathbf{v}^{(j)}, \mathbf{f}^{(j)}, \boldsymbol{\Theta}^{(j)}) \right] + \mathbb{E}_j \left[ \log p(\mathbf{v}^{(j)} \mid \boldsymbol{\Theta}^{(j)}) - \log q(\mathbf{v}^{(j)}) \right] \right)}_{\text{(I) Likelihood and partition term}} \\ &\quad - \underbrace{\sum_{j=1}^J \text{KL}(q(\mathbf{r}^{(j)}) \parallel p(\mathbf{r}^{(j)}))}_{\text{(II) Function prior regularization}} - \underbrace{\text{KL}(q(\mathbf{R}) \parallel p(\mathbf{R} \mid \boldsymbol{\Theta}_W))}_{\text{(III) Projection prior regularization}}.\end{aligned}\tag{26}$$

The first group (I) corresponds to the expected local data likelihood and latent-indicator partition term, the second group (II) regularizes each region’s inducing variable posterior toward its GP prior, and the third group (III) penalizes deviation of the global projection posterior  $q(\mathbf{R})$  from its GP prior parameterized by  $\boldsymbol{\Theta}_W$ .

### (I) Likelihood term: details for a fixed region $j$

The conditional likelihood is

$$\log p(\mathbf{y}^{(j)} \mid \mathbf{f}^{(j)}, \mathbf{v}^{(j)}) = \sum_{i \in \mathcal{D}_n^{(j)}} \left[ v_i^{(j)} \log \mathcal{N}(y_i^{(j)} \mid f_i^{(j)}, \sigma_j^2) + (1 - v_i^{(j)}) \log \frac{1}{u_j} \right].$$

**GP conditional for  $\mathbf{f}^{(j)}$ .** With local inducing variables  $\mathbf{r}^{(j)}$  (standardized outputs) and projection  $W_j$ , the conditional prior is

$$p(\mathbf{f}^{(j)} \mid \mathbf{r}^{(j)}, W_j) = \mathcal{N}\left(\mathbf{K}_{fr}^{(j)} (\mathbf{K}_r^{(j)})^{-1} \mathbf{r}^{(j)}, a_{m(j)} \mathbf{C}_{nn}^{(j)} - \mathbf{K}_{fr}^{(j)} (\mathbf{K}_r^{(j)})^{-1} \mathbf{K}_{rf}^{(j)}\right),$$

where  $[\mathbf{K}_{fr}^{(j)}]_{i\ell} = a_{m(j)} C(\|W_j \mathbf{x}_i^{(j)} - \bar{\mathbf{z}}_\ell^{(j)}\|^2)$  and  $\mathbf{C}_{nn}^{(j)}$  is built from projected local inputs  $\{W_j \mathbf{x}_i^{(j)}\}$ .

For each  $i$ ,

$$\begin{aligned}\mathbb{E}[f_i^{(j)} \mid \mathbf{r}^{(j)}, W_j] &= \mathbf{K}_{fr}^{(i,j)} (\mathbf{K}_r^{(j)})^{-1} \mathbf{r}^{(j)}, \\ \text{Var}(f_i^{(j)} \mid \mathbf{r}^{(j)}, W_j) &= a_{m(j)} - \mathbf{K}_{fr}^{(i,j)} (\mathbf{K}_r^{(j)})^{-1} \mathbf{K}_{rf}^{(i,j)}.\end{aligned}$$

Taking expectation over  $q(\mathbf{r}^{(j)})$  and  $q(W_j)$  gives

$$\begin{aligned}\mathbb{E}[f_i^{(j)}] &= \mathbb{E}_{q(W_j)} [\mathbf{K}_{fr}^{(i,j)}] (\mathbf{K}_r^{(j)})^{-1} \boldsymbol{\mu}_r^{(j)}, \\ \mathbb{E}[(f_i^{(j)})^2] &= \mathbb{E}_{q(W_j)} [\text{Var}(f_i^{(j)} \mid \mathbf{r}^{(j)}, W_j)] + \mathbb{E}_{q(W_j)} [(\mathbf{K}_{fr}^{(i,j)} (\mathbf{K}_r^{(j)})^{-1} \boldsymbol{\mu}_r^{(j)})^2] \\ &\quad + \text{tr}\left(\mathbb{E}_{q(W_j)} [\mathbf{K}_{fr}^{(i,j)} (\mathbf{K}_r^{(j)})^{-1} \mathbf{K}_{rf}^{(i,j)}] (\mathbf{K}_r^{(j)})^{-1} \boldsymbol{\Sigma}_r^{(j)}\right).\end{aligned}$$

**Closed forms via kernel expectations.** Introduce

$$\Psi_1^{(j)} = \mathbb{E}_{q(\mathbf{W}_j)}[\mathbf{K}_{fr}^{(j)}] \in \mathbb{R}^{n \times L_1}, \quad \Psi_2^{(i,j)} = \mathbb{E}_{q(\mathbf{W}_j)}[\mathbf{K}_{rf}^{(i,j)} \mathbf{K}_{fr}^{(i,j)}] \in \mathbb{R}^{L_1 \times L_1}.$$

Assuming a squared-exponential correlation  $C(\|\cdot\|) = \exp(-\frac{1}{2}\|\cdot\|^2)$  and a mean-field Gaussian marginal for the entries of  $\mathbf{W}_j$ ,

$$q(w_{kd}^{(j)}) = \mathcal{N}(\mu_{kd}^{(j)}, (\sigma_{kd}^{(j)})^2),$$

the  $(i, \ell)$  entry of  $\Psi_1^{(j)}$  admits

$$[\Psi_1^{(j)}]_{i\ell} = a_{m(j)} \prod_{k=1}^K \frac{1}{\sqrt{1 + (\mathbf{x}_i^{(j)})^\top \boldsymbol{\Sigma}_k^{(j)} \mathbf{x}_i^{(j)}}} \exp\left(-\frac{((\boldsymbol{\mu}_k^{(j)})^\top \mathbf{x}_i^{(j)} - \bar{z}_{\ell k}^{(j)})^2}{2[1 + (\mathbf{x}_i^{(j)})^\top \boldsymbol{\Sigma}_k^{(j)} \mathbf{x}_i^{(j)}]}\right)$$

where  $\boldsymbol{\mu}_k^{(j)} \in \mathbb{R}^D$  is the mean vector of row  $k$  of  $\mathbf{W}_j$  and  $\boldsymbol{\Sigma}_k^{(j)} = \text{diag}((\sigma_{k1}^{(j)})^2, \dots, (\sigma_{kD}^{(j)})^2)$  is its diagonal covariance under  $q(\mathbf{W}_j)$ . Similarly, for  $\Psi_2^{(i,j)}$ ,

$$[\Psi_2^{(i,j)}]_{\ell\ell'} = a_{m(j)}^2 \exp\left(-\frac{1}{2}\|\bar{\mathbf{z}}_\ell^{(j)} - \bar{\mathbf{z}}_{\ell'}^{(j)}\|^2\right) \prod_{k=1}^K \frac{1}{\sqrt{1 + 2(\mathbf{x}_i^{(j)})^\top \boldsymbol{\Sigma}_k^{(j)} \mathbf{x}_i^{(j)}}} \exp\left(-\frac{((\boldsymbol{\mu}_k^{(j)})^\top \mathbf{x}_i^{(j)} - \bar{z}_k^{(j)})^2}{1 + 2(\mathbf{x}_i^{(j)})^\top \boldsymbol{\Sigma}_k^{(j)} \mathbf{x}_i^{(j)}}\right)$$

with  $\bar{\mathbf{z}} = (\bar{\mathbf{z}}_\ell^{(j)} + \bar{\mathbf{z}}_{\ell'}^{(j)})/2$  and  $\bar{z}_k$  its  $k$ th component. The detailed derivation could be seen in Appendix (AUEB et al., 2013).

**Convenient scalars.** For each  $(j, i)$  define

$$\begin{aligned} V_{1,j,i} &:= a_{m(j)} - \text{tr}\left((\mathbf{K}_r^{(j)})^{-1} \Psi_2^{(i,j)}\right), \\ T_{2,j,i} &:= \text{tr}\left((\mathbf{K}_r^{(j)})^{-1} \Psi_2^{(i,j)} (\mathbf{K}_r^{(j)})^{-1} (\boldsymbol{\mu}_r^{(j)} \boldsymbol{\mu}_r^{(j)\top} + \boldsymbol{\Sigma}_r^{(j)})\right), \\ E_{f,j,i} &:= [\Psi_1^{(j)} (\mathbf{K}_r^{(j)})^{-1} \boldsymbol{\mu}_r^{(j)}]_i, \\ \text{quad}_{j,i} &:= \frac{(y_i^{(j)})^2 - 2y_i^{(j)} E_{f,j,i} + V_{1,j,i} + T_{2,j,i}}{2\sigma_j^2}. \end{aligned}$$

Then the expected conditional log-likelihood contribution equals

$$\sum_{i \in \mathcal{D}_n^{(j)}} \rho_i^{(j)} \left(-\frac{1}{2} \log(2\pi\sigma_j^2) - \text{quad}_{j,i}\right).$$

## (II) Partitioning expectations

For the logistic prior  $p(v_i^{(j)} = 1 \mid \mathbf{x}_i^{(j)}, \mathbf{W}_j, \mathbf{v}_j) = \sigma(\xi_i^{(j)})$ , with  $\xi_i^{(j)} = \mathbf{v}_j^\top [1, \mathbf{W}_j \mathbf{x}_i^{(j)}]$ , we need

$$\sum_{i \in \mathcal{D}_n^{(j)}} \mathbb{E}_{q(\mathbf{W}_j)q(\mathbf{v}^{(j)})} \log \frac{p(v_i^{(j)} \mid \mathbf{x}_i^{(j)}, \mathbf{W}_j, \mathbf{v}_j)}{q(v_i^{(j)})}.$$

Under the mean-field Gaussian  $q(\mathbf{W}_j)$  above,

$$\mu_{z,i}^{(j)} = v_{0,j} + \sum_{k=1}^K \sum_{d=1}^D v_{k,j} \mu_{kd}^{(j)} x_{i,d}^{(j)}, \quad (\sigma_{z,i}^{(j)})^2 = \sum_{k=1}^K \sum_{d=1}^D (v_{k,j} x_{i,d}^{(j)})^2 (\sigma_{kd}^{(j)})^2.$$

Hence  $z_i^{(j)} \sim \mathcal{N}(\mu_{z,i}^{(j)}, (\sigma_{z,i}^{(j)})^2)$ . The expectations  $\mathbb{E}[\log \sigma(z_i^{(j)})]$  and  $\mathbb{E}[\log(1 - \sigma(z_i^{(j)}))]$  are computed by Gaussian–Hermite quadrature:

$$\int_{-\infty}^{\infty} e^{-x^2} f(x) dx \approx \sum_{t=1}^{n_q} w_t f(x_t),$$

where  $x_t$  are roots of  $H_{n_q}(x)$  and the weights are  $w_t = \frac{2^{n_q-1} n_q! \sqrt{\pi}}{n_q^2 [H_{n_q-1}(x_t)]^2}$ .

### (I)+(II) Summary and optimal $q(v)$

Define, for each  $(i, j)$ ,

$$T_1^{i,j} = -\frac{1}{2} \log(2\pi\sigma_j^2) - \text{quad}_{j,i} + \mathbb{E}_{q(\mathbf{w}_j)} \log \sigma(\mathbf{v}_j^\top [1, \mathbf{W}_j \mathbf{x}_i^{(j)}]),$$

$$T_2^{i,j} = -\log u_j + \mathbb{E}_{q(\mathbf{w}_j)} \log(1 - \sigma(\mathbf{v}_j^\top [1, \mathbf{W}_j \mathbf{x}_i^{(j)}])).$$

Then

$$\sum_{i \in \mathcal{D}_n^{(j)}} \left[ \rho_i^{(j)} T_1^{i,j} + (1 - \rho_i^{(j)}) T_2^{i,j} - \rho_i^{(j)} \log \rho_i^{(j)} - (1 - \rho_i^{(j)}) \log(1 - \rho_i^{(j)}) \right].$$

Optimizing w.r.t.  $\rho_i^{(j)}$  yields

$$\rho_i^{(j)} = \frac{e^{T_1^{i,j}}}{e^{T_1^{i,j}} + e^{T_2^{i,j}}}, \quad \text{and} \quad \sum_{i \in \mathcal{D}_n^{(j)}} \log(e^{T_1^{i,j}} + e^{T_2^{i,j}}).$$

### (III) KL divergence for the global inducing variables $\mathbf{R}$

From the prior in the main text,

$$p(\mathbf{R}) = \prod_{k=1}^K \prod_{d=1}^D \mathcal{N}(\mathbf{R}_{:kd} | \mathbf{0}, \mathbf{K}_R^{(k)}), \quad [\mathbf{K}_R^{(k)}]_{\ell\ell'} = s^2 \exp\left(-\frac{\|\tilde{\mathbf{x}}_\ell - \tilde{\mathbf{x}}_{\ell'}\|^2}{2\ell_{w,k}^2}\right).$$

Our *per-element* mean-field posterior is

$$q(\mathbf{R}) = \prod_{\ell,k,d} \mathcal{N}(R_{\ell,k,d} | \mu_{\ell kd}, \sigma_{\ell kd}^2) \equiv \prod_{k,d} \mathcal{N}(\boldsymbol{\mu}_{kd}, \boldsymbol{\Sigma}_{kd}),$$

where  $\boldsymbol{\mu}_{kd} = [\mu_{1kd}, \dots, \mu_{L_2 kd}]^\top$  and  $\boldsymbol{\Sigma}_{kd} = \text{diag}(\sigma_{1kd}^2, \dots, \sigma_{L_2 kd}^2)$ . Hence, for each  $(k, d)$ ,

$$\text{KL}(q(\mathbf{R}_{:kd}) \| p(\mathbf{R}_{:kd})) = \frac{1}{2} \left[ \log \frac{|\mathbf{K}_{RR}^{(k)}|}{|\boldsymbol{\Sigma}_{kd}|} - L_2 + \text{tr}((\mathbf{K}_{RR}^{(k)})^{-1} \boldsymbol{\Sigma}_{kd}) + \boldsymbol{\mu}_{kd}^\top (\mathbf{K}_{RR}^{(k)})^{-1} \boldsymbol{\mu}_{kd} \right].$$

Summing over all  $(k, d)$  gives the projection prior penalty  $\text{KL}(q(\mathbf{R}) \| p(\mathbf{R}))$ .

**Implicit marginal  $q(\mathbf{W}_j)$ .** Since  $q(\mathbf{R})$  is Gaussian and  $p(\mathbf{W} | \mathbf{R})$  is a linear–Gaussian conditional GP, the induced marginal  $q(\mathbf{W})$  is Gaussian. In practice, we only need the first two moments of  $q(\mathbf{W}_j)$  (entering  $\Psi_1^{(j)}$  and  $\Psi_2^{(i,j)}$ ), which are computed analytically from the conditional GP moments and the diagonal  $q(\mathbf{R})$  above; the resulting formulas agree with the row-wise mean/variance parameters  $\{\mu_{kd}^{(j)}, (\sigma_{kd}^{(j)})^2\}$  used in (I)–(II).

### Putting it together and optimization details

Combining (I)–(III) over  $j = 1, \dots, J$  yields the full ELBO  $\mathcal{L}$ . All expectations of  $\log \sigma(\cdot)$  are computed by Gaussian–Hermite quadrature with degree  $n_q$ ; all remaining expectations are closed-form under the Gaussian assumptions above. We maximize  $\mathcal{L}$  by stochastic gradient ascent with respect to

$$\{\boldsymbol{\mu}_r^{(j)}, \boldsymbol{\Sigma}_r^{(j)}\}_{j=1}^J, \quad \{\mu_{\ell kd}, \sigma_{\ell kd}\}_{\ell,k,d}, \quad \tilde{\mathbf{x}} = (\tilde{\mathbf{x}}_\ell)_{\ell=1}^{L_2}, \quad \text{and } \{\mathbf{v}_j, u_j, \sigma_j, \mu_{m(j)}, a_{m(j)}\}_{j=1}^J, \quad s, \{\ell_{w,k}\}_{k=1}^K.$$

We enforce positivity of variance/lengthscale parameters by optimizing in the log-domain. Gradients are obtained by automatic differentiation (e.g., PyTorch).